seas using the pore density of denitrifying benthic foraminifera Anjaly Govindankutty Menon^{1*}, Aaron L. Bieler^{2, 3}, Hanna Firrincieli¹, Rachel Alcorn⁴, Niko Lahajnar^{1, 6} Catherine V. Davis⁴, Ralf Schiebel², Dirk Nürnberg⁵, Gerhard Schmiedl^{1, 6}, Nicolaas ¹Department of Earth System Sciences, Institute for Geology, Universität Hamburg, Bundesstrasse 55, D - 20146 Hamburg, Germany ²Climate Geochemistry Department Max Planck Institute for Chemistry, Hahn-Meitner-Weg 1, D - 55128 Mainz, Germany ³Department of Earth and Planetary Sciences, ETH Zürich, Sonneggstrasse 5, 8092 Zürich, Switzerland ⁴Department of Marine, Earth, and Atmospheric Sciences, North Carolina State University, 2800 Faucette Dr, Raleigh, NC, 27607, United States ⁵GEOMAR Helmholtz Centre for Ocean Research Kiel, Wischhofstr. 1-3, Geb. 8c, Raum 106, D-24148 Kiel, Germany ⁶Center for Earth System Research and Sustainability, Institute for Geology, Universität Hamburg, Bundesstrasse 55, D-20146 Hamburg, Germany *Corresponding author: anjalygmenon9@gmail.com.govindankutty.menon@uni-hamburg.de

Quantitative reconstruction of deglacial bottom-water nitrate in marginal Pacific

Abstract

Quantifying past ocean nitrate concentrations is crucial for understanding the global nitrogen cycle. Here, we reconstruct deglacial bottom-water nitrate concentrations ([NO₃-]_{BW}) reconstruction—in the oxygen-deficient zones of the Sea of Okhotsk, the Gulf of California, the Mexican Margin, and the Gulf of Guayaquil. Using the pore density of denitrifying benthic foraminifera as a nitrate proxy, differences in [NO₃-]_{BW} are observed at the study sites spanning the Last Glacial Maximum to the Holocene. Changes in water-column denitrification, water-mass ventilation, primary productivity, and sea surface temperatures may account for nitrate differences at the study sites. The [NO₃-]_{BW} in the Sea of Okhotsk, the Gulf of California, and the Gulf of Guayaquil are influenced by the intermediate water masses while, the [NO₃-]_{BW} at the Mexican Margin is likely influenced by deglacial changes in the Pacific Deep Water. The comparison of past and present [NO₃-] shows that the modern Gulf of Guayaquil and the Gulf of California currently have stronger oxygen-deficient zones with higher denitrification than during the Last Glacial Maximum. In contrast, the modern Mexican Margin and the Sea of Okhotsk may have higher oxygen than during the Last Glacial Maximum, indicated by low modern denitrification.

1. Introduction

75

76

77 The marine nitrogen cycle is a complex web of microbially mediated processes controlling the 78 inventory and distribution of bioavailable nitrogen in marine environments (Casciotti, 2016). 79 Biological nitrogen fixation by nitrogen-fixing diazotrophs (e.g., cyanobacteria) in the surface 80 layer is the main source of bioavailable nitrogen in the ocean, and denitrification and anammox, 81 are the main fixed nitrogen loss processes (Lam and Kuypers, 2011), both of which occur under low-oxygen conditions. The primary form of bioavailable nitrogen in the ocean is nitrate (NO₃-), 82 83 (Casciotti 2016), which is a limiting nutrient throughout the tropical and subtropical oceans (Moore et al., 2013). 84 Oxygen-deficient zones (ODZs) are regions of very low dissolved oxygen (O2) where the O2 85 concentration is less than 22 µmol/kg, usually within depths of 100-1,200 m (Levin, 2003; 2018). 86 Oxygen plays a key role in the marine nitrogen cycle (Keeling et al., 2010) because some microbial 87 88 processes require oxygen while others are inhibited by it (Voss et al., 2013). For example, 89 denitrification (reduction of nitrate to dinitrogen gas) in the ocean occurs only in suboxic (oxygen 90 <5μmol/kg) conditions (Codispoti et al., 2001; Levin, 2018). On a global scale, ~30-50% of fixed nitrogen loss in the world's oceans occurs in ODZs (Gruber, 2008), either through denitrification 91 92 or anammox (Devol et al., 2006; Lam and Kuypers, 2011; Evans et al., 2023). Due to the complex interactions and feedbacks within the biogeochemical nitrogen cycle, the amount of benthic 93 94 denitrification also influences other important processes, such as global nitrogen fixation and net primary production (Somes et al., 2017; Li et al., 2024). Benthic denitrification plays an important 95 role in shaping global nitrogen fixation, and net primary production (Somes et al., 2017; Li et al., 96 97 2024). Oxygen Deficient Zones ODZs cover only 1% of the world's seafloor (Codispoti et al., 98 2001), however, 10% of the global benthic denitrification occurs in these regions (Bohlen et al., 99 2012). Observations and climate model simulations have predicted that ODZs will continue to expand until at least the year 2100 (Stramma et al., 2008, 2010; Schmidtko et al., 2017; Oschlies, 100 101 2021). However, the long-term evolution of ODZs remains uncertain (Yamamoto et al., 2015; Takano et al., 2018; Fu et al., 2018; Frölicher et al., 2020). There is growing evidence that ODZs 102 103 may contract during transient and equilibrium climate warmings over timescales of millennia and 104 beyond (Auderset et al., 2022; Moretti et al., 2024). Observations and climate model simulations 105 predicted the expansion of ODZs (Stramma et al., 2008, 2010; Schmidtko et al., 2017; Oschlies,

2021) to continue at least until the year of 2100. However, the evolution of ODZs on timescales of hundreds to thousands of years remains uncertain (Yamamoto et al., 2015; Takano et al., 2018, Fu et al., 2018; Frölicher et al., 2020). Considering the role of ODZs in modulating the marine nitrogen cycle, it is of key scientific interest to understand how nitrogen cycling works in these ecosystems and the potential factors that influence the nitrogen cycle. In this study, we use the pore density (number of pores per unit area) of Bolivina spissa and Bolivina subadvena as a NO₃- proxy (Fig. 1 (a)) to reconstruct bottom-water nitrate [NO₃-]_{BW} in intermediate water depths of the Sea of Okhotsk, the Gulf of California, the Gulf of Guayaquil, and in the Pacific Deep Water (PDW) depths of the Mexican Margin (Fig. 2 and 3). The [NO₃]_{BW} calibration using the pore density of B. spissa and B. subadvena (see Fig. 1 (b)) developed in Govindankutty Menon et al. (2023) is applied in the current study. Combining a proxy for [NO₃]_{BW} (pore density of denitrifying foraminifera) and a proxy for N-cycle processes in the water column (δ^{15} N_{bulk}) facilitates a more comprehensive understanding of past N-cycling in different zones of the water column. Here, we try to understand 1) whether there are differences in reconstructed [NO₃]_{BW} between today, deglacial, and glacial periods in the four studied sites, and 2) whether the reconstructed [NO₃]_{BW} records are in agreement with insights drawn from δ¹⁵N_{bulk} data.

123 <u>1.1 Application of δ¹⁵N_{bulk} and its potential limitations</u>

The stable isotope signature of nitrogen in the sedimentary organic matter (δ^{15} N_{bulk}) is an established proxy for water-column denitrification and for understanding changes associated with nutrient utilization (Thunell et al., 2004; Robinson et al., 2009; Martinez and Robinson, 2010; Dubois et al., 2011, 2014; Tesdal et al., 2013; Wang et al., 2019; Riechelson et al., 2024). An increase (or decrease) in nutrient availability in relation to nutrient demand results in an increase (or decrease) in δ^{15} N values (Wada and Hattori, 1978; Montoya, 1990). When the oxygen in the ocean is depleted, either due to global warming or increased remineralization, denitrification rates in the water column are also increasing and so is δ^{15} N (Wang et al., 2019). When oxygen supply in the ocean is reduced, either due to global warming or increased availability of organic matter for remineralization, sedimentary δ^{15} N increases alongside intensified water column denitrification (Wang et al., 2019). Therefore, δ^{15} N_{bulk} can be an important tool for reconstructing past changes in denitrification in the ODZs. During the last glacial period, δ^{15} N_{bulk} measurements suggest that

136 denitrification rates within ODZs increased from the Last Glacial Maximum (LGM) to the Holocene (Robinson et al., 2009, Martinez and Robinson, 2010). 137 138 The δ¹⁵N records from the bulk sediment can be subject to interlinked processes/or sources which can complicate their interpretation. The 815 Noulk records from the whole sediment can be subject to 139 140 various processes/or sources which can complicate their interpretation. For example, diagenetic alteration during sinking in the water column and burial in the sediment (Altabet and Francois, 141 142 1994; Lourey et al., 2003), as well as terrestrial or shelf sources of organic and inorganic nitrogen 143 (Schubert & Calvert, 2001; Kienast et al., 2005; Meckler et al., 2011), and remotely advected water masses with different δ¹⁵N values (for e.g., Southern Californian margin; Liu and Kaplan, 1989), 144 could influence the δ^{15} N signatures in sediments. Nevertheless, Tesdal et al. (2013) proposed that 145 $\delta^{15}N_{bulk}$ can be a reliable indicator for individual locations reflecting the oceanographic conditions 146 147 of the surrounding environments. 148 Foraminifera are unicellular eukaryotes that are abundant in marine environments (Goldstein, 1999), and can be either planktic or benthic. The nitrogen isotopes of organic matter bound and 149 protected within the calcite shell of planktic foraminifera ($\delta^{15}N_{FB}$) are less subjected to diagenesis 150 or sedimentary contamination than $\delta_{2}^{15}N_{bulk}$ and can be used to understand major nitrogen 151 152 transformations occurring in the ocean (Ren et al., 2012; Studer et al., 2021). There are well-153 documented disagreements between bulk sediment $\delta^{15}N$ and foraminifera-bound $\delta^{15}N$ records, particularly in glacial-interglacial comparisons (Studer et al., 2021). While δ^{15} N_{bulk} suggests strong 154 variability in water-column denitrification between the LGM and deglaciation, δ¹⁵N_{FB} records 155 indicate a more moderate change, with a peak during deglaciation but relatively stable values 156 during the LGM and Holocene. This highlights that $\delta^{15}N_{bulk}$ and $\delta^{15}N_{FB}$ may reflect different 157 aspects of the nitrogen cycle (Studer et al., 2021). The nitrogen isotopes of organic matter bound 158 159 and protected within the calcite shell of planktic foraminifera ($\delta^{15}N_{FB}$) are less subjected to 160 diagenesis or sedimentary contamination and can be used to understand major nitrogen transformations occurring in the ocean (Ren et al., 2012; Studer et al., 2021). Recent studies 161 (Auderset et al., 2022; Hess et al., 2023; Moretti et al., 2024) based on $\delta^{15}N_{FB}$ have shown that 162 163 water column denitrification decreased and ODZs contracted during warmer-than-present periods of the Cenozoic (Auderset et al., 2022; Hess et al., 2023; Moretti et al., 2024). Another study based 164 on 815N_{FB} (Studer et al., 2021) suggests that water column denitrification was at its peak during 165 the deglaciation but was comparable during the LGM and the Holocene in the Eastern Equatorial 166

Formatted: Superscript

Formatted: Superscript

Formatted: Subscript

Formatted: Superscript

Formatted: Subscript

 $\delta^{15}N_{bulk}$ values over the Holocene is related to a decrease in Southern Ocean nutrient utilization 168 169 and not due to a decrease in denitrification. Other studies (Ganeshram et al., 2002; Deutsch et al., 170 2004; Eugster et al., 2013) have shown that reactive nitrogen inventories were elevated during 171 glacial periods, largely due to reduced denitrification in the water column and sediments. 172 1.2 Pore density of benthic foraminifera as a bottom-water nitrate proxy 173 Foraminifera account for a major part of benthic denitrification in the ODZs (up to 100% in some 174 environments) (Piña-Ochoa et al., 2010a; 2010b; Glock et al., 2013; Dale et al., 2016, Chocquel et 175 al., 2021, Rakshit et al., 2025). Benthic foraminifera are responsible for a large fraction of benthic 176 denitrification in ODZs (Piña Ochoa et al., 2010a; 2010b; Glock et al., 2013; Dale et al., 2016). 177 Some species, for example B. spissa, which are Some species for example; Bolivina spissa which 178 are abundant in ODZs in and around the Pacific Ocean (Glock et al., 2011; Fontanier et al., 2014) 179 can use NO₃⁻ as an electron acceptor (see Fig. 1 (a)) and thus can denitrify (Risgaard-Petersen 180 2006; Piña-Ochoa et al., 2010a; 2010b). 181 A study by Glock et al. (2019) proposed for some denitrifying foraminifera, denitrification is their preferred respiration pathway. The uptake of NO₃ by these foraminifera is likely through pores in 182 the test (see Fig. 1 (a)). Nitrate is completely denitrified to dinitrogen gas (N2) partly by the 183 foraminifera themselves (Risgaard-Petersen 2006; Woehle and Roy et al., 2018; Orsi et al., 2020; 184 185 Gomaa et al., 2021), and partly supported by prokaryotic endobionts (Bernhard et al., 2012a, 186 Woehle and Roy et al., 2022). 187 To date, benthic foraminifera are the only eukaryote holobiont known to perform complete 188 heterotrophic denitrification (Risgaard-Petersen 2006; Kamp et al., 2015). Every *Bolivina* species 189 tested so far (including Bolivina seminuda), can denitrify (Piña-Ochoa et al., 2010a; Bernhard et 190 al., 2012b), suggesting that denitrification is a common survival strategy of Bolivinidae under 191 oxygen-depleted conditions (Glock et al., 2019). This makes species of this genus particularly 192 suitable candidates for reconstructing past nitrate levels using pore characteristics as a proxy. Every 193 Bolivina species tested so far (including Bolivina seminuda), can denitrify (Piña Ochoa et al., 194 2010a; Bernhard et al., 2012b), suggesting that denitrification is a common survival strategy of 195 Bolivinidae under oxygen depleted conditions (Glock et al., 2019). In low-oxygen environments, 196 such as the ODZs off Peru, Costa Rica, and the hypoxic Sagami Bay, B. spissa increase their pore 197 density with decreasing ambient NO₃ availability (Govindankutty Menon et al., 2023). Thus, their

Pacific. In contrast, Riechelson et al. (2024) used $\delta^{15}N_{\text{bulk}}$ and hypothesized that the decrease in

167

Formatted: Font: Italic

Formatted: Font: Italic

Formatted: Font: Italic

Formatted: Font: Italic

pore density of several *Bolivina* species, such as *B. spissa*, and *B. subadvena*, is significantly, linearly correlated with bottom water nitrate concentrations (see Fig. 1 (b)) in their habitat (Glock et al., 2011; Govindankutty Menon et al., 2023) is an empirically calibrated proxy that shows the strongest correlation with the bottom-water nitrate concentration (see Fig. 1 (b)) in their habitat (Glock et al., 2011; Govindankutty Menon et al., 2023) rather than bottom-water oxygen, temperature, water depth, salinity or pore water nitrate. Therefore, the pore density of several *Bolivina* species such as *B. spissa*, and *B. subadvena* is a promising empirical proxy for paleo-NO₃ reconstruction (Glock et al., 2018; Govindankutty Menon et al., 2023).

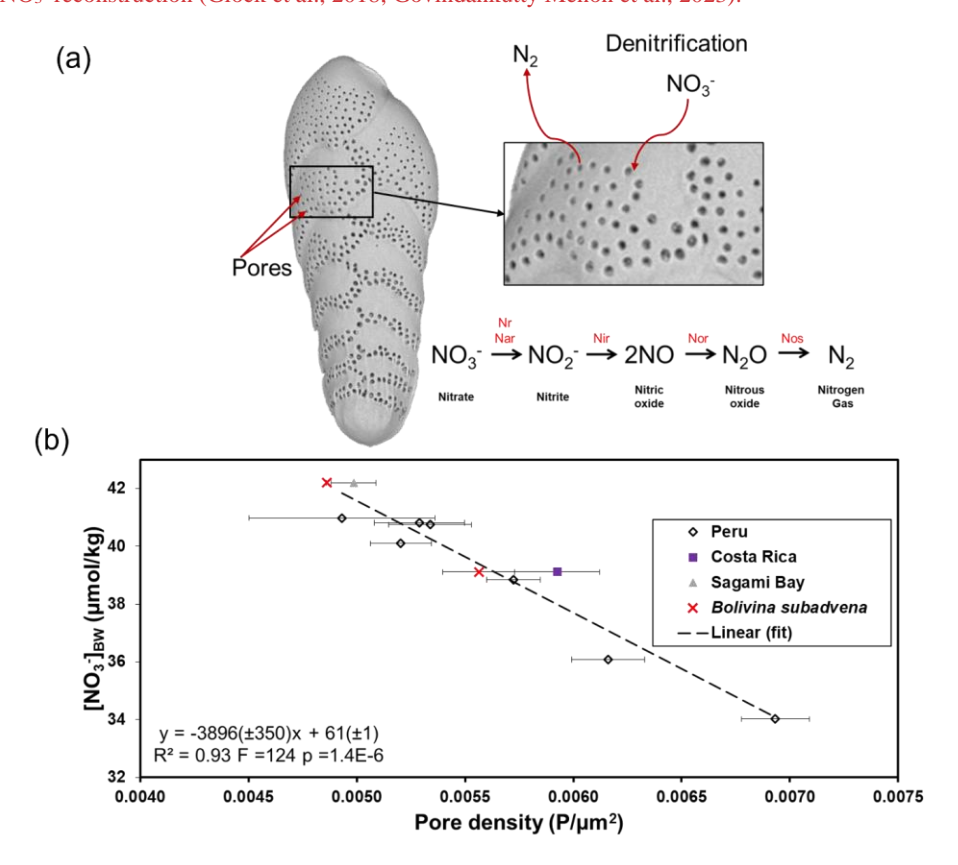
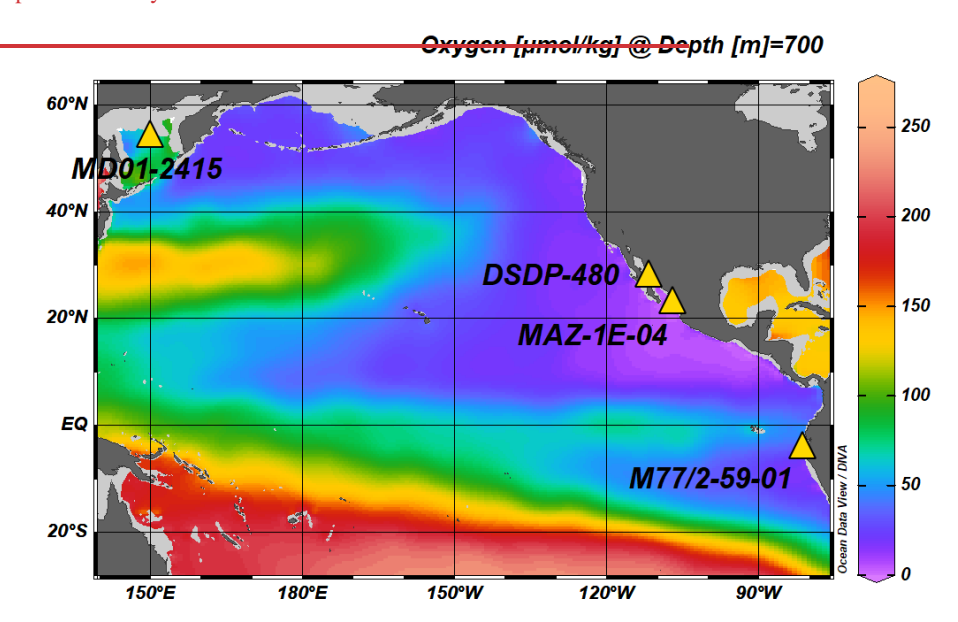


Figure 1: The (a) schematic view of nitrate (NO_3^-) uptake, and the excretion of nitrogen gas (N_2) by the benthic foraminifera *Bolivina spissa*. The step-wise denitrification pathway from NO_3^- to N_2^- involving enzymes such as nitrate reductase (Nr Nar), nitrite reductase (Nir), nitric-oxide

reductase (Nor), and nitrous oxide reductase (Nos) is also shown. (b) Correlation between pore density of *Bolivina spissa* from Peru, off Costa Rica, Sagami Bay, and *Bolivina subadvena* with bottom-water nitrate [NO₃]_{BW} from Govindankutty Menon et al. (2023). <u>If no species name is indicated in the legend, the analysed species was *B. spissa*. The error bars are 1 standard error of the mean.</u>

In this study, we use the pore density (number of pores per unit area) of *B. spissa* and *B. subadvena* as a NO₃-proxy (Govindankutty Menon et al., 2023) to reconstruct [NO₃-]_{Bw}-in intermediate water depths of the Sea of Okhotsk, the Gulf of California, the Gulf of Guayaquil, and in the Pacific Deep Water (PDW) depths of the Mexican Margin (Fig. 2 and 3). The [NO₃-]_{Bw} calibration using the pore density of *B. spissa* and *B. subadvena* (see Fig. 1 (b)) developed in Govindankutty Menon et al. (2023) is applied in the current study. Combining a proxy for bottom-water nitrate [NO₃-]_{Bw} (pore density of denitrifying foraminifera) and a proxy for N-cycle processes in the water column (8¹⁵N_{bulk}) might facilitate a more comprehensive understanding of past N-cycling in different zones of the water column. Here, we try to understand whether 1) there are differences in reconstructed [NO₃-]_{Bw}-between glacial and deglacial periods in the four studied sites, 2) the reconstructed [NO₃-]_{Bw}-records are in agreement with 8¹⁵N_{bulk} data, and 3) there was more or less NO₃- in the past than today.



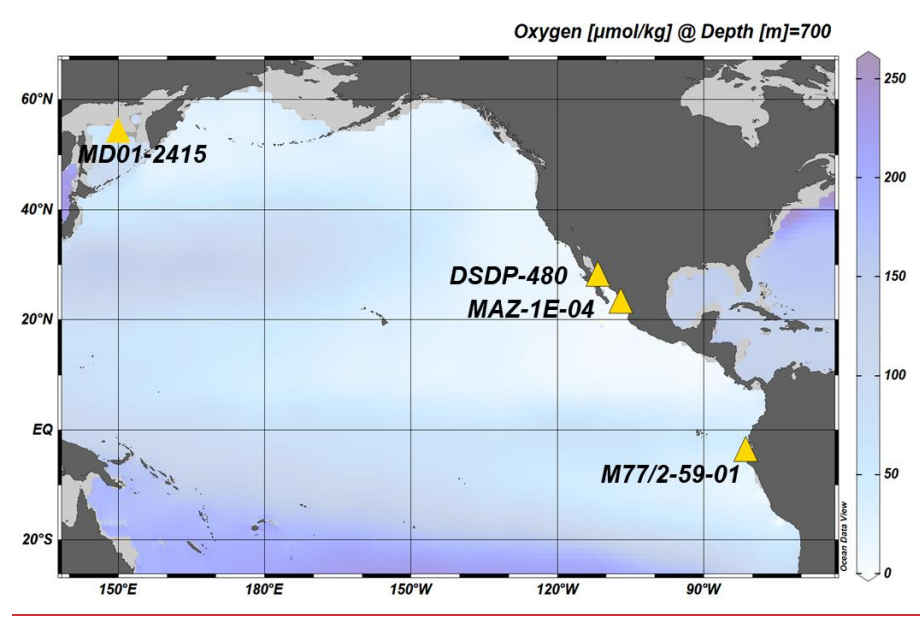
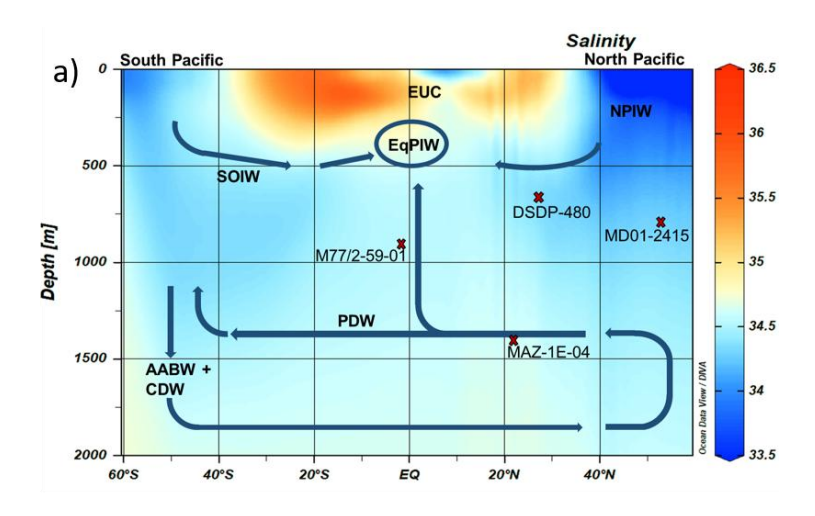


Figure 2. Location of sediment cores used in the current study and mean annual oxygen concentrations at 700 m depth (Garcia et al., 2019). Sediment cores are indicated by yellow triangles: Sea of Okhotsk (core MD01-2415; water depth: 822 m), Gulf of California (DSDP Site-480; water depth: 747 m), Mexican Margin (core MAZ-1E-04; water depth: 1463 m), and Gulf of Guayaquil (core M77/2-59-01; water depth: 997 m). Map created with Ocean Data View (Schlitzer, R., 2023).



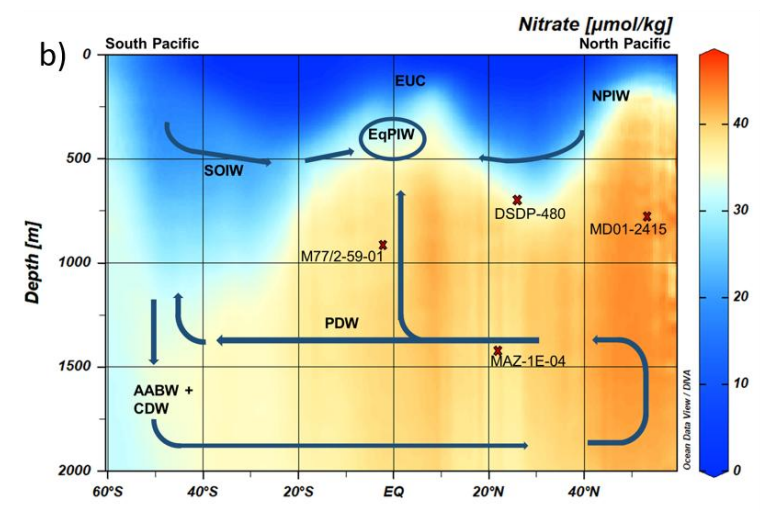


Figure 3. Modern a) salinity and b) nitrate distribution along a N-S transect across the Pacific (Garcia et al., 2019) with major subsurface and deep-water masses (blue arrows) and formation areas of North Pacific Intermediate Water (NPIW) and Southern Ocean Intermediate Water (SOIW) are included. Sediment cores used for $[NO_3^-]_{BW}$ reconstruction are shown (red crosses) projected to the N-S hydrographic transect. Equatorial Pacific Intermediate Water (EqPIW), Equatorial Undercurrent (EUC), NPIW, SOIW, Pacific Deep Water (PDW), Antarctic Bottom Water (AABW), and Circumpolar Deep Water (CDW). Profiles generated by Ocean Data View (Schlitzer, R., 2023) using the data from World Ocean Atlas 2018 (Garcia et al., 2019).

2. Materials and methods

- 2.1 Study area and sampling of sediment cores. We used downcore samples from the Eastern Tropical South Pacific, ETSP (Gulf of Guayaquil (M77/2-59-01), Eastern Tropical North Pacific the ETNP (Mexican Margin, MAZ-1E-04), the Gulf of California (Guaymas Basin, DSDP-64-480), and the Sea of Okhotsk (MD01-2415), over the last ~20,000 years (Fig. 3). The Gulf of Guayaquil sediment core M77/2-59-01 (03°57.01' S, 81°19.23' W, recovery 13.59 m) was collected from the northern edge of the ODZ at a water depth of 997 m during the RV Meteor cruise M77/2 in 2008 (Mollier-Vogel et al., 2013, 2019; Nürnberg et al., 2015). The piston core MAZ-1E-04, Mexican Margin (22.9°N, 106.91°W) was collected on board the RV El Puma at a water depth of 1463 m. The CALYPSO giant piston core MD01-2415 (53°57.09' N, 149°57.52' E, recovery 46.23 m) was recovered from the northern slope of the Sea of Okhotsk at 822 m water depth during the WEPAMA cruise MD122 of the R-V Marion Dufresne (Holbourn et al., 2002;
- W) from the Gulf of California was retrieved at a water depth of 747 m close to the Guaymas

 Basin. For details on the sampling procedure of foraminiferal specimens, please refer to the

 Supplementary Methods section in the Supplementary Information.

Nürnberg & Tiedemann, 2004). The Deep-Sea Drilling Project core DSDP- 480 (27°54' N, 111°39'

- 2.2 Sampling of foraminiferal specimens for the quantitative nitrate record. A total of 1541 fossil specimens of *B. spissa* (number of specimens, n =1268) and *B. subadvena* (n = 273) were used for the [NO₃⁻]_{BW}-reconstructions across the four sites. A total of 37 sample depths (n = 669) from the Gulf of Guayaquil (M77/2-059-1), 23 sample depths (n = 455) from the Mexican Margin (MAZ-1E-04), 16 sample depths (n = 273) from the Gulf of California (DSDP-480), 11 sample depths (n=144) from the Sea of Okhotsk (MD01-2415) were utilized. Porosity measurements were made on 6-20 well-preserved specimens of *B. spissa* and *B. subadvena* in each sample. The sediment samples were washed and wet sieved through a 63 μm mesh sieve. The residues were dried in an oven at 38-50°C. The samples were sieved into the grain-size fractions of 63-125, >125-250, >250-315, >315-355, >355-400, and >400 μm. Specimens of *B. spissa*, and *B. subadvena* were picked from the 125-250 μm fraction.
- 2.3-2 Automated image analysis. All specimens of *B. spissa* and *B. subadvena* were imaged using
 a Scanning Electron Microscope (Hitachi Tabletop SEM TM4000 series) at Hamburg University,
 Germany with an accelerating voltage of 15 kV using a back-scattered electron (BSE) detector

(Further methodological details are provided in the Supplementary Information). The specimens were not sputter coated to allow for future geochemical analyses. For porosity measurements, the total area on the first (oldest) ten chambers (equivalent to an area of 50,000 to 70,000 μm²) was measured using the ZEN 3.4 blue edition software. Size normalization was done to minimize the impact of ontogenetic effects on the pore density. The pore parameters such as the pore density (PD), mean pore size, and porosity were determined with the automated image analyzing software AmiraTM 3D pro using a previously trained deep learning algorithm. The deep learning algorithm that was used for this study is included in the Amira software package. The deep learning algorithm was initially trained with manually segmented pores on 52 images of *B. spissa* and 60 images of *B. subadvena*. Only those specimens that had a total area equivalent to at least 50,000 μm² were used for the automated analysis. Data from smaller specimens that did not fit within the minimal total area were discarded. The detailed methodology of the porosity measurements and trained deep learning algorithm is described in Govindankutty Menon et al. (2023).

Following the image analysis, pore density data of benthic foraminifera from the four ODZs were used for the quantitative reconstruction of [NO₃⁻]_{BW} (Fig. 64). We distinguished five different time intervals, including the Last Glacial Maximum (LGM; 22–17 ka BP), Heinrich Stadial 1 (H1; 17–15 ka BP), Bølling - Allerød (BA; 14.7-12. 9 ka BP), Younger Dryas (YD; 12.9–11.7 ka BP), Early Holocene (EH; 11.7–8.2 ka BP) and Middle to Late Holocene (MLH; 8–0 ka BP) to describe the [NO₃⁻]_{BW} in the East Pacific and the Sea of Okhotsk (Fig. 6). We present updated chronostratigraphies of the studied cores, primarily based on accelerator mass spectrometry (AMS) radiocarbon (¹⁴C) dating, as detailed in the Supplementary Information.

The [NO₃⁻]_{BW} from all cores were calculated using the calibration equation;

$$[NO_3^-]_{BW} = -3896 (\pm 350) PD + 61(\pm 1)$$
 (1)

where PD is the pore density of benthic foraminifera (Govindankutty Menon et al., 2023).

303 The standard error of the mean (SEM) for one sample was calculated using the equation;

$$SEM_{[NO_3^-]_{BW}} = \frac{SD_{[NO_3^-]_{BW}}}{\sqrt{n}}$$
 (2)

where n is the number of specimens analyzed in each sample and SD is 1 standard deviation of mean reconstructed [NO₃-]_{BW}.

$$SD_{[NO_3^-]_{BW}} = \sqrt{(350 \ X \ PD)^2 + (-3896 \ X \ SD_{PD})^2 + (1)^2}$$
 (3)

Formatted: English (United States)

Formatted: Line spacing: 1.5 lines

A complete error propagation was done for the calculation of the errors of the reconstructed [NO₃⁻]BW including both the uncertainty of the mean PD within the samples and the uncertainties of the calibration function. The reconstructed [NO₃⁻]_{BW} and the calculated SEM and SD of each sample are shown in the Supplementary files. 2.4 Optimization of age models We here present updated chronostratigraphies of cores studied, mainly based on accelerator mass spectrometry (AMS) radiocarbon (14C) datings. Sea of Okhotsk: We used the age tie points and 14C ages published by Bubenshchikova et al. (2015); based on Nürnberg and Tiedemann, (2004) for the age model of core MD01-2415. The accelerator mass spectrometry (AMS) 14C dates were incorporated in between the age tie points to minimize the age uncertainty. For the current study, the age depth model was updated using Marine 20 (Heaton et al., 2020) within the Bchron package (Haslett & Parnell, 2008) in RStudio (RStudio Team, 2023) with a local DeltaR of 546 years from the Davydov Cape (Kuzmin et al., 2007). Gulf of California: We used raw 14C ages of planktic foraminifera from Keigwin and Jones (1990) for updating the age-depth model for DSDP Site 480, Radiocarbon age calibration was done using Marine20 with a local DeltaR of 301 years from the Guaymas Basin (Goodfriend and Flessa, 1997). The Behron package was used for determining the age-depth model and calibrating the age. Mexican Margin: The age model for core MAZ-1E-04 has been entirely built in the framework of the current study. We used planktic foraminifera Globigerinoides ruber, Globigerinoides bulloides, Trilobatus sacculifer for the AMS 14 C dating, Approximately 200 tests of these species were selected from the 125-250 μm fraction. The radiocarbon measurements of planktic foraminifera were carried out at the Alfred Wegener Institute (AWI) in Bremerhaven, Germany using the MICADAS system and at the National Ocean Sciences Accelerator Mass Spectrometry Facility, USA. We applied a manual continuous Marine Reservoir Age (MRA) correction using the MRAs from the closest available location to the core MAZ-1E-04 from the published literature (Butzin et al., 2020). Then the corresponding MRAs were subtracted from the raw 14C ages of planktic foraminifers to achieve the atmospheric 14C age. Radiocarbon age calibration was done

308

309 310

311

313

314

315

316 317

318

319 320

321

322 323

324

325

326

327 328

329

330

331

332

333

334

335 336 Formatted: Line spacing: Multiple 1.08 li

using Intcal20 (Reimer et al., 2020) in the Behron package in RStudio.

337 Gulf of Guayaquil: The published age model of core M77/2-59-01 (Mollier-Vogel et al., 2019) is

338 based on ten AMS 14C ages measured using planktic foraminifera species Neogloboquadrina

dutertrei at the Leibniz Laboratory at Kiel University, Germany. For the current study, the age-

depth model was updated using Marine20 in the Behron package (Haslett & Parnell, 2008) in

341 RStudio with a DeltaR of 200 ± 50 years (Mollier-Vogel et al., 2013).

All information used for developing and updating the age models are shown in the Supplementary

343 files.

2.5-3 Sedimentary nitrogen isotope ($\delta^{15}N_{bulk}$) measurements. We have measured sedimentary nitrogen isotope ($\delta^{15}N_{bulk}$) rather than $\delta^{15}N_{FB}$ from cores taken from the Sea of Okhotsk, and Gulf of California, because the low abundances of foraminifera were utilized for other analysis. The analysis of bulk sediments allows for high-resolution records. Prior to the $\delta^{15}N_{bulk}$ measurements, the Total Nitrogen (TN%) content of 20 sediment samples from the Sea of Okhotsk and 54 samples from the Gulf of California were measured at the Institute for Geology, Hamburg University, Germany using a flash combustion method with a Eurovector EA-3000 analyzer. The $\delta^{15}N_{bulk}$ measurements for both the Sea of Okhotsk and the Gulf of California were accomplished at the Max Planck Institute for Chemistry (Mainz), Germany using a DELTA V ADVANTAGE Isotope Ratio Mass Spectrometer (IRMS) equipped with a FLASH 2000 Organic Elemental Analyzer. The results were expressed in standard δ -notation (equation 4). The standard deviation (\pm SD) of all individual analysis runs based on a certified international reference standard (USGS65) and internal laboratory standards (L-Phenylalanine and L-Glutamic acid) referenced to certified international reference standards was < 0.3%. The $\delta^{15}N_{bulk}$ data for the Sea of Okhotsk and the Gulf of California are shown in Supplementary Table ST1.

$$\delta^{15}N(\%_0) = \left[(^{15}N:^{14}N_{\text{sample}})^{15}N:^{14}N_{\text{air}} \right] - 1 \times 1,000$$
 (4)

For the Gulf of Guayaquil core M77/2-59-01, the $\delta^{15}N_{bulk}$ data published by Mollier-Vogel et al. (2019) was used. Their measurements were done on ~ 5 –50 mg of homogenized and freeze-dried bulk sediments using a Carlo-Erba CN analyzer 2500 interfaced directly to a Micromass-Isoprime mass spectrometer at Bordeaux University. Results are expressed in standard δ -notation (equation 4) relative to atmospheric dinitrogen gas (N_2).

2.6-4 Nitrate offset to present conditions. The reconstructed $[NO_3^-]_{BW}$ from each location is subtracted from the modern $[NO_3^-]$ present at the respective locations from similar water depths the cores were retrieved from. This provided the $[NO_3^-]$ offset which is the difference ($\Delta[NO_3^-]$ (μM)) between the modern $[NO_3^-]$ and the past reconstructed $[NO_3^-]_{BW}$. The modern $[NO_3^-]$ for each location was taken from World Ocean Atlas 2018 (Garcia et al., 2019). The details are given in Table 1 supplementary information.

Table 1. Site location information of modern [NO₃⁻] taken for the nitrate offset from World Ocean Atlas 2018.

Locations	Latitude	Longitude	Water depth	Station ID	[NO ₃ ⁻]
			(m)		(µmol/kg)
Gulf of Guayaquil,	3.5° S	81.5°W	1050	21457 (B)	42.5
(M77/2-59-01)					
Mexican Margin,	21.5°N	106.5°W	1450	27910 (B)	42.75
(MAZ-1E-04)					
Sea of Okhotsk,	53.5°N	149.5°E	850	33729 (B)	43.4
(MDO1-2415)					
Gulf of California,	27.5°N	111.5°W	750	29197 (B)	35.3
(DSDP, 480)					

2.7 Organic carbon accumulation rates. Organic carbon accumulation rates for cores from the Sea of Okhotsk, the Gulf of California, and the Gulf of Guayaquil were calculated using the sedimentary total organic carbon weight percentage, sediment dry bulk density, and sedimentation rates (equation 5).

TOC Accumulation rate = Sedimentation rate × sediment dry bulk density × TOC (wt%) (5)

The sedimentation rates were calculated from the age depth model that has been updated within this study. The total organic carbon content and dry bulk densities were taken from Bubenshchikova et al. (2015) for the Sea of Okhotsk, Leclaire and Kerry (1982) for the Gulf of

382 California, and Mollier Vogel et al. (2019) for the Gulf of Guayaguil. Organic carbon data was not available for core MAZ-1E-04 from the Mexican Margin. High resolution dry bulk densities 383 384 were not available for DSDP Site 480 from the Gulf of California. For this core, dry bulk densities have been calculated using the wet dry bulk density and porosity of the sediment shown in figure 385 24 of Curray et al. (1982). Since the resulting dry bulk data resolution for this core was very sparse 386 for each depth in the core, the dry bulk density of the closest data point was used. There was a 387 388 large data gap between the 2 m and 9 m sediment depth, with a considerable jump in the dry bulk 389 density between these two sampling depths. Thus, between these two data points, dry bulk densities were linearly interpolated. The data for the organic carbon accumulation rate is given in 390 391 the Supplementary files.

2.8 Statistical analysis. The statistical analyses presented in this paper were carried out using RStudio. The t test was used to test for the significant difference between datasets of unequal sample sizes after carrying out an initial variance test. The confidence interval of 95% (p < 0.05) was set for the significance test.

396 3. Results

Holocene.

392 393

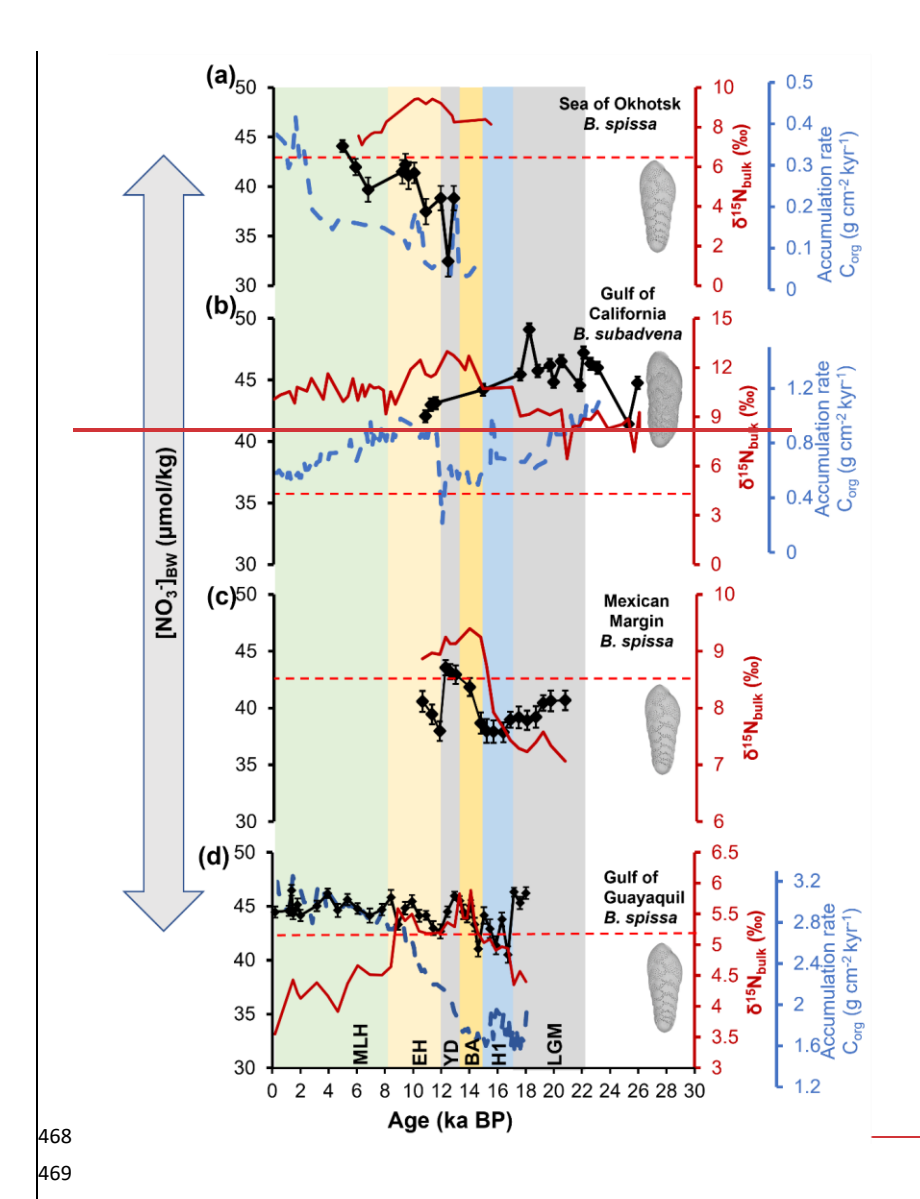
394 395

- We reconstructed deglacial [NO₃]_{BW} using downcore sediment samples from the Sea of Okhotsk
 (MD01-2415), the Gulf of California (DSDP- 480), the Mexican Margin (MAZ-1E-04), and the
 Gulf of Guayaquil (M77/2-59-01). The reconstructed [NO₃]_{BW} was compared to δ¹⁵N_{bulk} records
 of all cores (Fig. 4). All data records presented cover the time period starting from the Last Glacial
 Maximum, except for the core from the Sea of Okhotsk, which covers the late deglacial to the
- 403 3.1 Sea of Okhotsk (MD01-2415). The Sea of Okhotsk core MD01-2415 covers the Younger 404 Dryas, (YD, 12.8 ka BP) until the Middle to Late Holocene (MLH, 4.9 ka BP). The reconstructed 405 [NO₃]_{BW} values range from 32.8 µmol/kg to 44.1 µmol/kg (Fig. 4a). A gradual increase in [NO₃]_{BW} is observed from the Younger Dryas to the Middle to Late Holocene. At the beginning 406 of the Younger Dryas at 12.8 ka BP, [NO₃]_{BW} were relatively high and then decreased to a 407 408 minimum value of 32.8 μmol/kg at 12.4 ka BP. Since then, [NO₃]_{BW} steadily increased until the Middle to Late Holocene (MLH, 44.1 µmol/kg) (Fig. 4a). The [NO₃]_{BW} during the Middle to Late 409 Holocene (mean = $41.2 \mu \text{mol/kg}$) is significantly (t-test, p = 0.023) higher than during the Younger 410 Dryas (mean = 36.7 μ mol/kg). The sedimentary δ^{15} N_{bulk} record covers the interval from the Late 411

Heinrich Stadial 1 (H1, 15.4 ka BP) to the Middle Holocene (6.1 ka BP). The δ^{15} N_{bulk} values were 412 relatively high ranging from 7.1% to 9.4% with an average of 8.7%. The $\delta^{15}N_{bulk}$ values increased 413 414 steadily from the Late Heinrich Stadial 1 (15.4 ka BP) to the Early Holocene (EH, 10 ka BP) with higher values centered between the Late Younger Dryas (11.9 ka BP) and the beginning of the 415 Early Holocene. Since then, the $\delta^{15}N_{\text{bulk}}$ values decreased until the Middle to Late Holocene. 416 **3.2 Gulf of California (DSDP-480)**. The analyzed sections of DSDP Site 480 covered the Last 417 418 Glacial Maximum (22 ka BP) until the Early Holocene (10.8 ka BP). The reconstructed [NO₃]_{BW} ranged from 41.4 µmol/kg to 49.1 µmol/kg. The highest [NO₃⁻]_{BW} of 49.1 µmol/kg occurred 419 during the Last Glacial Maximum (18.2 ka BP). The data points from the Early Holocene (11.6-420 10.8 ka BP) were the only Holocene data from this core providing the lowest [NO₃⁻]_{BW} estimate 421 of 42.1 µmol/kg during the Early Holocene (10.8 ka BP) (Fig. 4b). A distinct difference in 422 423 [NO₃]_{BW} between the glacial period (mean = 46.1 µmol/kg) and the Early Holocene (42.7 424 μmol/kg) was observed with [NO₃]_{BW} found to be substantially higher during the glacial period (t-test, p = 0.0067) (Fig. 4b). Accordingly, the [NO₃]_{BW} followed a decreasing pattern from the 425 glacial period to the Early Holocene. The $\delta^{15}N_{\text{bulk}}$ values varied between 6.4% and 13% with an 426 average of 10.2‰ (Fig. 4b). The δ¹⁵N_{bulk} values from the Guaymas Basin were similar to the 427 δ^{15} N_{bulk} values (average 9.6‰) of Pride (1997) and Altabet et al. (1999). During the last glacial 428 period, the δ^{15} N_{bulk} values were low ranging from 8.5% to 9%. At the onset of the deglaciation, 429 430 the δ^{15} N_{bulk} values increased by more than 2% with large-scale changes reaching a maximum of 13% during the Younger Dryas. Afterward, we observed a gradual decline in $\delta^{15}N_{\text{bulk}}$ values 431 432 throughout the Middle to Late Holocene (mean 10.7%) and this pattern continued to the present. 3.3 Mexican Margin (MAZ-1E-04). This core MAZ-1E-04 covered the Last Glacial Maximum 433 (20.5 ka BP) until the Early Holocene (10.47 ka BP). The [NO₃]_{BW} values range from 37.7 434 435 μ mol/kg to 43.5 μ mol/kg. We observed the highest $[NO_3^-]_{BW}$ during the Younger Dryas. From the beginning to the end of the Last Glacial Maximum, [NO₃]_{BW} followed a decreasing trend (Fig. 436 4c). The [NO₃⁻]_{BW} levels continued to steadily decrease until Heinrich Stadial 1 and consistently 437 stayed low throughout this period. There was a strong change in [NO₃⁻]_{BW} from the end of Heinrich 438 Stadial 1 to the end of Younger Dryas (Fig. 4c). We observed a peak in [NO₃]_{BW} from the 439 beginning of Bølling-Allerød, BA (14.29 ka BP) and it continued throughout the Younger Dryas 440 (Fig. 4c). Afterwards, [NO₃]_{BW} declined during the Early Holocene. The δ¹⁵N_{bulk} values taken 441

(Fig.4c). 3.4 Gulf of Guayaquil (M77/2-59-01). This core covered the Last Glacial Maximum (18 ka BP) until the Middle to Late Holocene (0.18 ka BP). The reconstructed [NO₃⁻]_{BW} values range from 40.5 μmol/kg to 46.5 μmol/kg. The highest [NO₃⁻]_{BW} occurred during the Last Glacial Maximum (Fig. 4d). The reconstructed $[NO_3]_{BW}$ levels during the Last Glacial Maximum (mean = 45.6 μmol/kg) were slightly higher than during the Middle to Late Holocene (mean = 44.9 μmol/kg) (t-test, p = 0.046). The δ^{15} N_{bulk} values were relatively low ranging between 4% and 6% (Fig. 4d). During the Last Glacial Maximum, the $\delta^{15}N_{\text{bulk}}$ values were low, varying between 4.4% and 4.6%, close to the typical mean range of dissolved nitrate in the ocean (Sigman et al., 1997). Subsequently, the $\delta^{15}N_{bulk}$ values increased from 16.7 ka BP (4.9%), where we observed a decline in [NO $_3$]_{BW} to 8.9 ka BP (5.6%). The highest $\delta^{15}N_{bulk}$ values centered at ~14 ka BP (5.9%). From 8.9 ka BP onwards, a long-term decrease in $\delta^{15}N_{bulk}$ (< 4.4‰) was observed until the Latest Holocene, consistent with higher [NO₃]_{BW} levels during the Holocene (Fig. 4d). Despite higher [NO₃]_{BW} levels, our reconstruction doesn't show any strong variations during the Holocene.

from Alcorn et al. (2025) followed an increasing trend from the glacial towards the deglacial period



Formatted: English (United States)

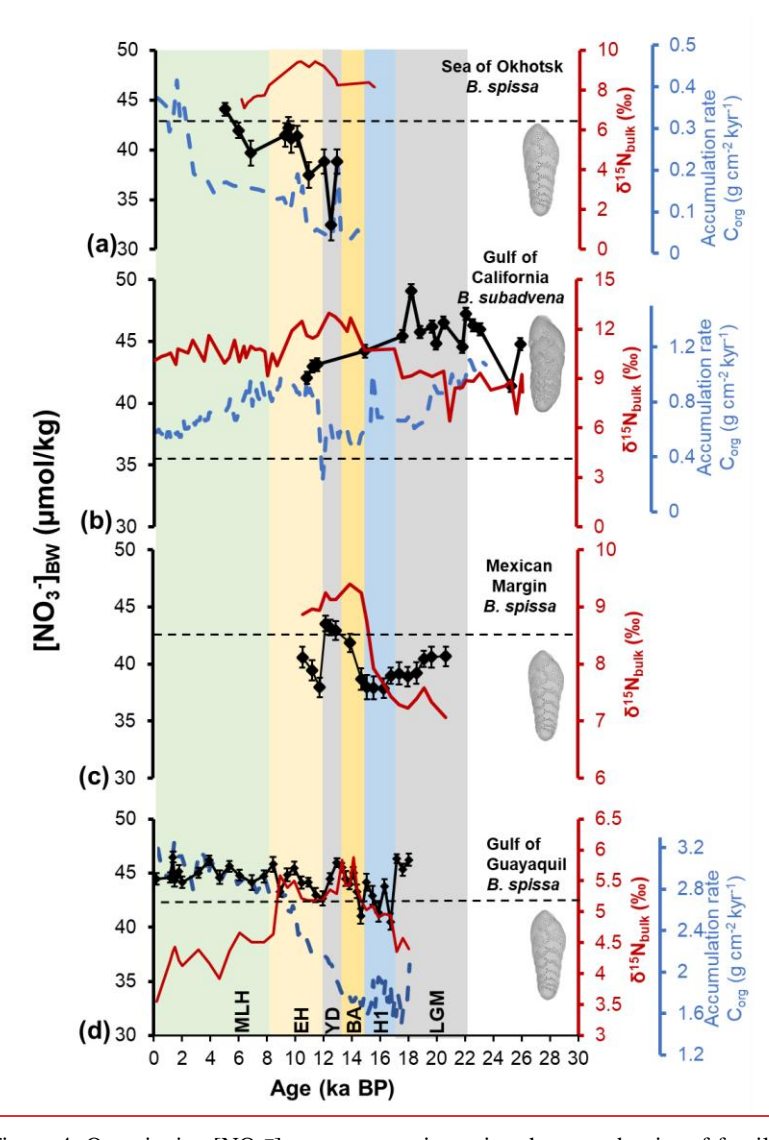


Figure 4. Quantitative [NO₃]_{BW} reconstruction using the pore density of fossil specimens of *B. spissa*, *B. subadvena* from a) the Sea of Okhotsk (MD01-2415), b) the Gulf of California (DSDP-480), c) the Mexican Margin (MAZ-1E-04), and d) Gulf of Guayaquil (M77/2-59-01). The sedimentary nitrogen isotope (δ^{15} N_{bulk}) records from the Sea of Okhotsk, and the Gulf of California are measured in this study, and the Gulf of Guayaquil is from Mollier-Vogel et al. (2019), and-

The $\delta^{15}N_{bulk}$ data for the Mexican Margin $\frac{\delta^{15}N_{bulk}}{\delta^{15}N_{bulk}}$ data is from Alcorn et al. (2025). The error bars of [NO₃–]_{BW} represent 1 SEM including a complete error propagation (using equations 3 and 4). The accumulation rate of total organic carbon (Supplementary files) calculated from published literature (Bubenshchikova et al., 2015; Leclaire & Kerry, 1982; Mollier-Vogel et al., 2019) is shown in blue dashed lines for the Sea of Okhotsk, the Gulf of California and the Gulf of Guayaquil cores respectively. The red-black dashed lines indicate the modern nitrate concentration of each location. Time intervals Middle to Late Holocene (MLH), Early Holocene (EH), Younger Dryas (YD), Bølling-Allerød (BA), Heinrich Stadial 1 (H1), and Last Glacial Maximum (LGM) are shown in the figure.

498'

 3.5 Comparing the nitrate offset ($\Delta[NO_3^-]$) between cores. To quantify the change in $[NO_3^-]_{BW}$ between past and present conditions, we calculated the difference ($\Delta[NO_3^-]$ (μM)) between the modern $[NO_3^-]$ (Garcia et al., 2019) and the reconstructed past $[NO_3^-]_{BW}$ for each core. A $\Delta[NO_3^-]$ value close to 0 implies that there is no offset to the modern value. A positive (or negative) $\Delta[NO_3^-]$ implies higher (or lower) values than today. The Gulf of California had the highest $\Delta[NO_3^-]$ values relative to the other cores (see Fig. 5), and none of the values are close to the modern values. In general, the $\Delta[NO_3^-]$ values in the Gulf of California and mostly in the Gulf of Guayaquil were positive (Fig. 5) which indicated that bottom water NO_3^- concentrations in the past were higher than today in these regions. The Mexican Margin and the Sea of Okhotsk had negative $\Delta[NO_3^-]$, implying that NO_3^- concentrations in the past were lower than today (Fig. 5)

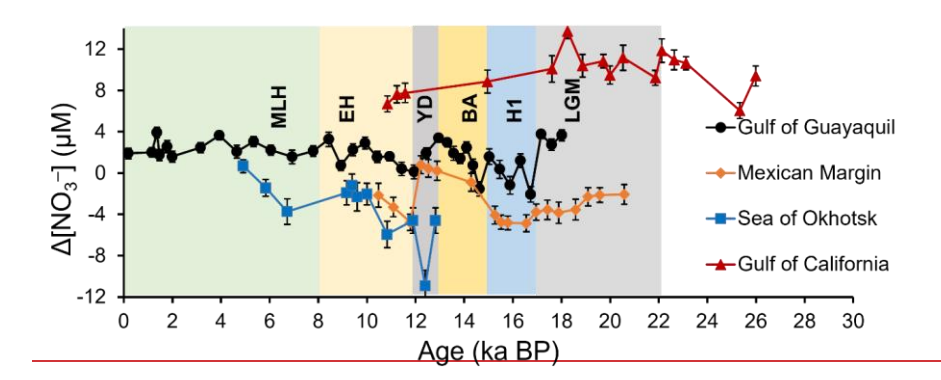


Figure 5. The nitrate offset (A[NO₃⁻] (µM)) revealing changes of bottom water nitrate concentrations over the last 30 kyrs. The [NO₃=l_{BW} were calculated from the pore density of the benthic foraminifera B. spissa and B. subadvena from all studied cores compared to modern NO₃⁻ concentrations at each location. The modern nitrate (Table 1 and see fig. 4) at the different locations has been taken from the World Ocean Atlas, 2018 (Garcia et al., 2019). Error bars represent 1 SEM.

4. Discussion

503

504 505

506

507

508 509 510

511

512

513

514

515

516

517

518 519

520

521

522 523

524

525

526 527

- Reconstruction of past [NO3] BW-in the ODZs is crucial for understanding the complex marine nitrogen cycle, and the processes/or factors involved in marine nutrient cycling. The comparison between past and modern NO3 - will provide a foresight on the ecological and environmental impacts of climate change in these regions. The pore density of benthic foraminifera represents a promising but still developing proxy for reconstructing past nitrate dynamics. Like most proxies based on biology, it reflects an indirect physiological response rather than a direct measure of nitrate. In addition, species-specific variability requires careful taxonomic control or its interpretation carries inherent limitations especially since not many records are available, yet, for this proxy. Thus, we used a multiproxy approach and combined it with $\delta^{15}N_{bulk}$, which provides a complementary perspective that strengthens reconstructions of nitrogen-cycling processes in oxygen-deficient zones.
- **4.1 Sea of Okhotsk.** Our data show that [NO₃⁻]_{BW} levels gradually increased through time and reached modern concentrations during the Middle-Holocene (Fig. 4a). Most of the nutrients in the northwestern Pacific including the Sea of Okhotsk are supplied by the upwelling of the North Pacific Deep Water (NPDW) (Gorbarenko et al., 2014). The weakened Kuroshio current (Ujiié and Ujiié, 1999) and increased sea ice extent (Ternois et al., 2001) weakened the upwelling of NPDW during the Last Glacial Maximum (LGM). Subsequent studies (Gray et al., 2020; Rae et al., 2020) have shown that the expansion of the North Pacific Gyre also resulted in less upwelling of NPDW during the LGM.
- 529
- During the LGM, the subpolar North Pacific was better ventilated at intermediate depths (Keigwin, 530
- 1998) and export productivity was reduced (Ternois et al., 2001; Narita et al., 2002; Seki et al., 531
- 2004). This is consistent with a strengthened meridional overturning circulation, with enhanced 532
- 533 formation of intermediate waters and advection of nutrient-depleted subtropical waters to high

latitudes (Rae et al., 2020). Furthermore, the North Pacific subpolar gyre extended ~3° further 534 south during the LGM (Gray et al., 2020), which shifted the westerly winds southward. This may 535 536 have resulted in less upwelling of the NPDW during the LGM. The prolonged ice cover with low biological productivity (Ternois et al., 2001; Narita et al., 2002; 537 538 Seki et al., 2004; Rae et al., 2020) and well-oxygenated water masses (Keigwin, 1998) might have prevented the formation of an oxygen deficient zone (ODZ) in the Sea of Okhotsk 539 (Bubenshchikova et al., 2015). This is supported by the absence of B. spissa, which are adapted to 540 living in dysoxic conditions, in our records during the LGM. 541 Deglacial low [NO₃]_{BW} which correspond to higher δ¹⁵N_{bulk} values (Fig. 4a) could be due to 542 enhanced primary productivity. It is important to note, however, that δ¹⁵N_{bulk} is influenced by 543 544 diagenetic alteration and the incorporation of allochthonous nitrogen, which can obscure the local 545 denitrification signal. Therefore, interpretations of $\delta^{15}N_{\text{bulk}}$ trends should be made cautiously and ideally corroborated with complementary proxies, such as foraminiferal pore density. Increased 546 547 nutrient supply from the Asian continental shelves and sea-ice retreat (Ternois et al., 2001) strengthened primary productivity. Indeed, the accumulation rate of total organic carbon was 548 relatively higher during the Younger Dryas (Bubenshchikova et al., 2015) in our core (Fig. 4a). 549 The increased oxygen demand and weakened ventilation of intermediate waters in the subarctic 550 Pacific (Lembke-Jene et al., 2018) gradually intensified the ODZ. These poorly oxygenated 551 552 conditions conceivably strengthened denitrification, resulting in low deglacial [NO₃⁻]_{BW} levels. 553 However, during the Middle to Late Holocene (MLH) a reorganization in atmospheric circulation favored enhanced formation of oxygenated North Pacific Intermediate Water (NPIW) (Wang et 554 al., 2020). Thus, mid-depth ventilation was closely associated with atmospheric circulation in the 555 Holocene and a weakened ODZ (Ohkushi et al., 2013; Bubenshchikova et al., 2015; Wang et al., 556 2020). These rising oxygen concentrations probably reduced denitrification (low $\delta^{15}N_{\text{bulk}}$) in the 557 558 Sea of Okhotsk, resulting in higher $[NO_3^-]_{BW}$ comparable to today's conditions (Fig. 4 & 5). The δ^{15} N_{bulk} values show a maximum from 13 ka to 10 ka BP, which indicates increased water-column 559 denitrification during that time. Nevertheless, the [NO₃]_{BW} increased during this time, which 560 indicates a decoupling from denitrification in the oxygen minimum in the water column and the 561 [NO₃]_{BW}. This could be related to the sea level rise during that time (Waelbroeck et al., 2008), 562 563 which increased the vertical distance of the sediments (i.e., bottom water) at the sampling site from

the center of denitrification.

4.2 Gulf of California. The Gulf of California ODZ is influenced by both intermediate and deepwater properties, similar to that of the open Pacific Ocean. Thus, the ODZ intensity in the Guaymas Basin is largely dependent on the oxygen content and ventilation of inflowing NPIW from the Sea of Okhotsk (Pride et al., 1999) and the demand for oxygen at depth. During the glacial period, the dissolved oxygen concentrations were higher due to better-ventilated NPIW at intermediate depths of the Northeast Pacific (Keigwin and Jones, 1990; Ganeshram et al., 1995; Keigwin 1998; Duplessy et al., 1988; Herguera et al., 2010; Cartapanis et al., 2011). Modeling studies show that the Laurentide and Cordilleran ice sheets increased in size (Benson et al., 2003), lowering the temperature of North America (Romanova et al., 2006) during the glacial period. The cold sinking air over the ice sheet established a semi-permanent high-pressure cell (Kutzbach & Wright Jr, 1985; Romanova et al., 2006) causing a substantially weaker North Pacific High (Ganeshram and Pedersen, 1998) or the southward displacement of the Inter Tropical Convergence Zone (Cheshire and Thurow, 2013). This resulted in a weak California Current along the coast and reduced upwelling-favorable winds (COHMAP et al., 1988; Cartapanis et al., 2011) along the North American coastline and reduced primary productivity (Ganeshram and Pedersen, 1998; Hendy et al., 2004; Cartapanis et al., 2011; Chang et al., 2015) within the ETNP and the Gulf of California during the glacial period. The nitrogen isotope ratios in the Guaymas Basin can be affected by subsurface denitrification in the Gulf and in the ETNP (Pride et al 1999). The increase in dissolved oxygen during the glacial period might have reduced water column denitrification (low δ^{15} N_{bulk}) thereby increasing the [NO₃⁻]_{BW} (Fig. 4b). Our study finds a declining trend in reconstructed [NO₃]_{BW} during the Early Holocene, slowly approaching modern concentrations. This coincides with a maximum in $\delta^{15}N_{\text{bulk}}$ values, suggesting elevated denitrification. This agrees with previous studies in the ETNP (Kienast et al., 2002) and within the Gulf of California (Pride et al., 1999), which showed that high denitrification most likely was associated with warming temperatures that occurred during this period. Furthermore, the scarcity of benthic foraminifera after the Early Holocene in our study coincides with laminations of the sediment core (Keigwin & Jones, 1990) below 10.8 ka BP, where reconstructed [NO₃]_{BW} begins to decrease. It is possible that redox conditions were too hostile for benthic foraminifers in the time periods when laminated sediments formed. We acknowledge limitations in our Holocene reconstruction due to the low abundance of B. subadvena and the limited calibration dataset available for this species, which may introduce a systematic offset (Govindankutty Menon et al.,

565

566 567

568

569

570 571

572

573

574 575

576

577

578

579

580

581

582 583

584

585

586

587 588

589

590

591 592

593 594

2023). *Bolivina subadvena* was used in this core due to the unavailability of *B. spissa*, and some values fall outside the existing calibration range. We also cannot rule out other factors influencing the proxy signal, such as microhabitat variability. Additional data and further proxy calibration are therefore essential to improve the robustness of Holocene bottom-water nitrate reconstructions.

599 600 601

602

603

604

605

606 607

608 609

610

611 612

613

614

615

616

617

618

619 620

621

622

623

624 625

626

596

597

598

4.3 Mexican Margin. Our study finds a steep rise in [NO₃]_{BW} between the Bølling-Allerød (BA) and the Younger Dryas (YD) (Fig. 4c). The transition period from the BA to the Holocene involved rapid oxygenation with increased oxygen levels at the onset of the YD (Jaccard & Galbraith, 2012; Ohkushi et al., 2013; Taylor et al., 2017). This has been linked to active ventilation by increased NPIW production at high latitudes in the North Pacific (Van Geen et al., 1996; Emmer and Thunell, 2000; Okazaki et al., 2010; Cartapanis et al., 2011; Chang et al., 2014). In addition, there was low primary productivity (Hendy et al., 2004; Pospelova et al., 2015), and a higher influx of freshwater (Broecker et al., 1985; Clark et al., 2002) during the YD. However, considering the deep location of the Mexican Margin core below the direct influence of intermediate water masses (Fig. 3), it is less likely to be reflected in the [NO₃⁻]_{BW}. Bulk sediment δ^{15} N records in the ETNP (Ganeshram et al., 1995; Pride et al., 1999; Emmer and Thunell, 2000; S. S. Kienast et al., 2002; Hendy et al., 2004) found a decrease in $\delta^{15}N_{bulk}$ during the YD due to reduced denitrification. Furthermore, a foraminifera-bound nitrogen isotope ($\delta^{15}N_{FB}$) study (Studer et al., 2021) in the eastern tropical Pacific also found a decrease in $\delta^{15}N_{FB}$ signatures during the Younger Dryas (Fig. 4c). In contrast to this, a bulk sediment δ^{15} N record of MAZ-1E-04 (Alcorn et al., 2025) depicts an increase in water column denitrification during the Younger Dryas. Thus, reduced denitrification may not be the dominant factor that led to the elevated [NO₃]_{BW} during this time. Instead, the Mexican Margin may be more influenced by the NO₃ variability from the Pacific Deep Water, PDW (see Fig. 3). Deep-sea reorganization and ventilation during the deglaciation may have influenced the [NO₃]_{BW}. At the onset of the deglaciation, deep Southern Ocean ventilation (reduced ¹⁴C ventilation ages) and atmospheric carbon dioxide (CO2) synchronously increased (Robinson et al., 2009; Burke and Robinson, 2012; Rae et al., 2018). This deglacial increase in ¹⁴C ventilation in the Pacific Ocean suggests that most of the increase in atmospheric CO2 is derived from old carbon in the Southern and Pacific Oceans (Rafter et al., 2022). The increase in reconstructed [NO₃⁻]_{BW} during the YD may thus reflect the release of sequestered nutrient- and carbon dioxide-rich waters during the deglaciation (Robinson et al., 2009; Rafter et al., 2022).

627 The relatively high [NO₃]_{BW} during the glacial period (Fig. 4c), before its decline in Heinrich Stadial 1, is likely indicative of reduced water-column denitrification (Ganeshram et al., 1995; 628 629 2000) due to reduced productivity (Ganeshram et al., 1995; Ganeshram and Pedersen, 1998) and low organic matter flux through the oxygen minimum zone (Ganeshram et al., 2000). In the ETNP, 630 631 including the Mexican Margin, coastal upwelling is driven by trade winds generated by subtropical high-pressure centers. These high-pressure centers largely result from differential heating of the 632 633 land and the ocean. As a result of glacial cooling on land, these high-pressure systems and the associated trade winds that drive the upwelling have likely been weakened (Ganeshram and 634 Pedersen, 1998). 635 4.4 Gulf of Guayaquil. The core M77/2-59-01 is in a region that is sensitive to changes in 636 subsurface denitrification in the ETSP (Robinson et al., 2007, 2009; Dubois et al., 2011, 2014). 637 638 The elevated reconstructed [NO₃]_{BW} levels (Fig. 4d) during the glacial period suggest decreased 639 water-column denitrification (Salvatteci et al., 2014; Erdem et al., 2020; Glock et al., 2022) and 640 relatively low local productivity (Ganeshram et al., 2000; Robinson et al 2007; 2009; Martinez and Robinson et al., 2010; Salvatteci et al., 2016). Nutrient export to the deep Southern Ocean 641 waters increased due to the sluggish Atlantic Meridional Overturning Circulation (Skinner et al., 642 2010), and increased atmospheric iron (Fe) deposition (Somes et al., 2017) during the glacial 643 period. This reduced the transport of preformed NO₃⁻ to the tropics via the Subantarctic Mode 644 645 Water (SAMW), limiting productivity. In fact, the total organic carbon (Fig. 4d) depicts low productivity during this period. Furthermore, the colder sea surface temperature (SST) and the 646 647 accelerated formation of SAMW and Antarctic Intermediate Water masses (Russell & Dickson, 2003; Galbraith et al., 2004) and the stronger high-latitude winds in the Southern Hemisphere 648 (Karstensen and Quadfasel, 2002) increased the ventilation rate (Meissner et al., 2005; Jaccard and 649 Galbraith, 2012; Muratli et al., 2010) during the glacial period. The resulting increased oxygen 650 651 concentrations (Robinson et al., 2005; Robinson et al., 2007) decreased the volume of ODZs, and nitrogen loss processes (lower δ^{15} N_{bulk} values, Fig. 4d) during the glacial period. In addition, 652 enhanced Fe deposition (Somes et al., 2017), and the glacial low sea level (Clark and Mix, 2002; 653 Wallmann et al., 2016), may have influenced the nitrate inventory in the tropical and subtropical 654 655 southern hemisphere. 656 A study by Glock et al. (2018) on core M77/2-52-2 from Peru applying the pore density of B. spissa also shows elevated [NO₃]_{BW} during the Last Glacial Maximum, a similar decline in [NO₃] 657

BW during the Heinrich Stadial 1 and thereafter a steady decrease in NO₃-BW throughout the 658 659 Holocene. 660 The deglacial decline in [NO₃] _{BW}, especially during Heinrich Stadial 1 in this study (Fig. 4d), indicates a gradual increase in surface productivity and bottom-water deoxygenation. High export 661 662 production strengthened the expansion of the ETSP ODZ during the deglaciation as compared to LGM and MLH (Salvatteci et al., 2016; Glock et al., 2018; Mollier-Vogel et al., 2019). This is 663 664 consistent with the denitrification signal in the Eastern Equatorial Pacific through westward advection from the Southeast Pacific margins (Martinez and Robinson, 2010). 665 The shift towards generally higher reconstructed [NO₃]_{BW} from the Middle-Holocene, (Fig. 4d), 666 implies a profound change in the climatic state of the Peruvian upwelling system and the associated 667 ODZ during this time. From the deglaciation toward the Late Holocene, there was a general 668 669 increase in productivity (Mollier-Vogel et al., 2019) as shown by organic carbon accumulation 670 rates (Fig. 4d). This increase in organic matter input and/or preservation was likely related to an increase in upwelling-driven delivery of nutrients towards the surface. The gradual decrease in 671 δ^{15} N_{bulk} values and higher [NO₃]_{BW} was likely related to a relaxation in nutrient utilization with a 672 nutrient supply exceeding the biological demand (Riechelson et al., 2024). Moreover, the core 673 674 M77/2-59-01 was retrieved outside of the core ODZ and is under the strong influence of the oxygen and nutrient-rich Equatorial Under Current subsurface waters (Salvatteci et al., 2019; Mollier-675 676 Vogel et al., 2019). These waters might have ventilated the Northern Peruvian margin and 677 deepened the oxycline at this site during the Middle-Holocene. Furthermore, enhanced zonal SST (Koutavas et al., 2006) and a northward shift of the ITCZ strengthened the Pacific Walker and 678 Hadley circulation during the Middle-Holocene across the tropical Pacific (Koutavas et al., 2006; 679 Mollier-Vogel et al., 2013; Salvatteci et al., 2019). These enhanced atmospheric circulations 680 681 brought oxygen-rich waters to intermediate depths off Peru via the equatorial subsurface 682 countercurrents (Koutavas et al., 2006; Mollier-Vogel et al., 2013; Salvatteci et al., 2019). Hence, 683 increased ventilation of subsurface water masses reduced the strength of nitrogen loss processes 684 and nutrient uptake during the MLH. 685 At present, the only quantitative reconstruction of bottom-water oxygen from these locations is the 686 core M77/2-59-01 from the Gulf of Guayaquil reported by Erdem et al. (2020). Their record 687 suggests a decline in bottom-water oxygen from the deglacial period to the Holocene. Future more detailed comparisons of the nitrate reconstructions with quantitative bottom water oxygen records 688

at the same cores will further improve our understanding about variability in redox conditions and nitrogen cycling.

4.5 Comparison of past and present [NO₃] at the studied locations. The [NO₃] during the present and past are compared to assess the resilience of our chosen study locations towards environmental and ecological impacts of climate change. The generally positive Δ[NO₃⁻] that we found (Fig. 54b) in the Gulf of California (Guaymas Basin) and the Gulf of Guayaquil indicate that today the [NO₃-] is lower than in the past. This suggests that today the nitrogen loss processes at these two core sites are stronger, most likely related to ocean warming and a decline in oxygen concentration of bottom waters. The Gulf of California core is within the heart of the oxygendeficient zone, and thus changes in ODZ oxygenation or denitrification will be more evident in this core than in any other core studied. Under nitrogen limitation, negative feedbacks (e.g., anammox) result in a decline in productivity (Naafs et al., 2019; Wallmann et al., 2022), which will stabilize the oxygen concentration. In the case of the Gulf of California, sediments are enriched in reactive iron (Fe) (Scholz et al., 2019). The decreasing NO₃-concentrations in the bottom water reduce the flux of NO₃ into the surface sediment. This leads to the release of sedimentary Fe, which enhances nitrogen fixation in the Guaymas Basin (Scholz et al., 2019). Thus, increased denitrification might not act as negative feedback in the Gulf of California because it might be countered by increased nitrogen fixation (White et al., 2013).

In the case of the Gulf of Guayaquil (Fig. 4d), whether today's elevated denitrification could enhance N_2 fixation also depends on the availability of Fe (Pennington et al., 2006). The primary productivity of the Peruvian ODZ is Fe limited due to the reduction of particular Fe oxides in shelf and slope sediments (Scholz et al., 2014). Modeling studies show that primary productivity will be amplified in the Peruvian ODZ due to the release of Fe from shelf and slope sediments (Wallmann et al., 2022). This may induce deoxygenation and drive the expansion and intensification of Peruvian ODZ resulting in a positive feedback loop, like in the Gulf of California. This situation is indicated by lower [NO₃-] today compared to the past ~20,000 years (Fig. 5).

The negative nitrate $\Delta[NO_3^-]$ in the Sea of Okhotsk and the Mexican Margin (Fig. 4a &c5) indicates that modern $[NO_3^-]$ levels are higher than in the reconstructed past. This suggests that modern nitrogen loss is decreased at these two core sites compared to the last deglaciation. The higher modern $[NO_3^-]$ in the Sea of Okhotsk is likely associated with less primary productivity and

more oxygen in the water column similar to the situation established in the MLH. The higher modern [NO₃-]_{BW} in the case of the Mexican Margin could be associated with sea level rise. The ODZ in the Mexican Continental Margin might have shifted to shallower depths today with less/or no benthic denitrification in intermediate water depths at the core site, resulting in high [NO₃-]_{BW} levels. During the glacial period, continental shelves were exposed due to sea-level lowstands (Clark and Mix, 2002; Kuhlmann et al., 2004; Wallmann et al., 2016), the main areas of primary productivity may have migrated offshore from the shallow shelf towards the continental slope relative to their Holocene positions. A similar situation occurred at the Benguela upwelling system during the LGM: TOC accumulation at the continental slope increased during the LGM in response to the seaward shift of centers of enhanced productivity (Mollenhauer et al., 2002). This offshore shift of the productivity centers and the most likely reduced remineralization rates, due to lower temperatures, indicate that the center of the ODZ at the Mexican Margin before sea level rise was possibly deeper than today. However, with the deglacial eustatic sea-level rise, the ODZ may have shifted to shallower depths. This shifted the main zone of denitrification further away from the seafloor, resulting in the increased modern [NO₃-]_{BW} in comparison to the LGM (Fig. 5).

5. Conclusion. The quantitative reconstruction of $[NO_3^-]_{BW}$ using the pore density of denitrifying benthic foraminifera over the last deglaciation at the four studied ODZs provides a comprehensive understanding of the past $[NO_3^-]$. Ocean deoxygenation and warming alter nutrient cycling and the functioning of marine ecosystems and food webs. Combining the relatively new pore density proxy of denitrifying foraminifera with $\delta^{15}N_{bulk}$ has the potential to further resolve the processes in the marine nitrogen cycle in oxygen deficient zones. The Gulf of Guayaquil and Gulf of California data shows elevated $[NO_3^-]_{BW}$ during the glacial period compared to deglacial and modern conditions. Considering the well-ventilated intermediate water masses in the Sea of Okhotsk, the Sea of Okhotsk may have also elevated $[NO_3^-]_{BW}$ in the glacial period. For the Mexican Margin core, $[NO_3^-]_{BW}$ was particularly strong during the Younger Dryas. The reconstructed $[NO_3^-]_{BW}$ from the Sea of Okhotsk, the Gulf of California, and the Gulf of Guayaquil are influenced by the formation of the North Pacific Intermediate Water. However, the $[NO_3^-]_{BW}$ in the deeper site, the Mexican Margin is likely influenced by the NO_3^- variability in Pacific Deep Water. The modern Gulf of Guayaquil and the Gulf of California have low $[NO_3^-]$ associated with increased denitrification and a strengthening ODZ. In contrast, higher modern $[NO_3^-]$ was

- 749 observed in the Sea of Okhotsk and the Mexican Margin, suggesting that these two study areas
- 750 have higher oxygen.
- 751 Code and Data availability
- 752 All data generated or analyzed during this study are included in the tables of this published article
- 753 (and its Supplementary information files) available in Supplementary information.
- 754 Author contributions
- 755 A.G.M wrote the core manuscript, did the sample preparation, electron microscopy, image and
- 756 statistical analyses of all the fossil foraminifera. N.G. planned the study design and sampling
- 757 strategy. G.S. hosted the research group, and provided access to SEM, and lab facilities at the
- 758 University of Hamburg, D.N. provided sampling material for cores MD01-2415 and M77/2-59-
- 759 01. C.D. provided sampling material for core MAZ-1E-04. N.L., R.S., and A.B. facilitated the
- measurement of nitrogen isotopes in the sediment samples of core MD01-2415 and DSDP-480.
- 761 R.A. contributed to the age model development of core MAZ-1E-04, and H.F helped in the image
- processing of core DSDP-480. All authors contributed to the discussion and preparation of the
- 763 manuscript.

769

- 764 Competing interests
- 765 The authors declare no competing interests.
- 766 Acknowledgements
- 767 We are grateful to the micropaleontology group at the University of Hamburg, Germany. We thank
- 768 Alfredo Martinez-Garcia, Max Planck Institute for Chemistry, Mainz, Germany for the support
 - with the measurement of nitrogen isotopes in the sediment samples. We acknowledge the help of
- 770 Jutta Richarz, Kaya Oda for lab support, PhD student Sven Brömme (Max Planck Institute for
- 771 Chemistry, Mainz) and student assistant Hannah Krüger. We thank Yvon Balut, Agnes Baltzer,
- 772 and the Shipboard Scientific Party of RV Marion Dufresne cruise WEPAMA 2001 for their kind
- 573 support. We thank IODP for providing the sample for core DSDP-480. The study is a contribution
- 774 to the Center for Earth System Research and Sustainability (CEN) of University of Hamburg.
 - Financial support

- 776 Funding was provided by the Deutsche Forschungsgemeinschaft (DFG) through both N.G.'s
- 777 Heisenberg grant GL 999/3-1 and grant GL 999/4-1. Funding for the core MD01-2415 recovery
- 778 was provided by the German Science Foundation (DFG) within project Ti240/11-1. The recovery
- 779 of core M77-59 recovery was a contribution of the German Science Foundation (DFG)
- 780 Collaborative Research Project "Climate-Biogeochemistry interactions in the Tropical Ocean"
- 781 (SFB 754).

References

782

783

784

785

786

787

788

789

790 791

792

793

794 795

796

797

798

799

800 801

802 803

804

805

806 807

808

809 810

811

812 813

814

815

816

817

- Alcorn, R. C., Ontiveros-Cuadras, J. F., Menon, A. G., Glock, N., Tappa, E. J., Burke, J., Cartapanis, O., & Davis, C. V.: Nonlinear Expansion of the Eastern Tropical North Pacific Oxygen Minimum Zone During the Last Deglaciation. Authorea Preprints, https://doi.org/10.22541/au.173335151.59466232/v1, 2025.
- Altabet, M. A., Pilskaln, C., Thunell, R., Pride, C., Sigman, D., Chavez, F., & Francois, R.: The nitrogen isotope biogeochemistry of sinking particles from the margin of the Eastern North Pacific. Deep Sea Research Part I: Oceanographic Research Papers, 46(4), 655-679, https://doi.org/10.1016/S0967-0637(98)00084-3, 1999.
- Altabet, M. A., & Francois, R. Sedimentary nitrogen isotopic ratio as a recorder for surface ocean nitrate utilization.: Global biogeochemical cycles, 8(1), 103-116, https://doi.org/10.1029/93GB03396, 1994.
- Auderset, A., Moretti, S., Taphorn, B., Ebner, P. R., Kast, E., Wang, X. T., ... & Martínez-García, A. Enhanced Ocean oxygenation during Cenozoic warm periods. Nature, 609(7925), 77-82, https://doi.org/10.1038/s41586-022-05017-0, 2022.
- Benson, L., Lund, S., Negrini, R., Linsley, B., & Zic, M. Response of north American Great basin lakes to Dansgaard–Oeschger oscillations. Quaternary Science Reviews, 22(21-22), 2239-2251, https://doi.org/10.1016/S0277-3791(03)00210-5, 2003.
- Bernhard, J. M., Edgcomb, V. P., Casciotti, K. L., McIlvin, M. R., & Beaudoin, D. J.: Denitrification likely catalyzed by endobionts in an allogromiid foraminifer. The ISME journal, 6(5), 951-960, https://doi.org/10.1038/ismej.2011.171, 2012a.
- Bernhard, J. et al. Potential importance of physiologically diverse benthic foraminifera in sedimentary nitrate storage and respiration. J. Geophys. Res. 117, https://doi.org/10.1029/2012JG001949, 2012b.
- Bohlen, L., Dale, A. W., & Wallmann, K.. Simple transfer functions for calculating benthic fixed nitrogen losses and C: N: P regeneration ratios in global biogeochemical models. *Global biogeochemical cycles*, 26(3), https://doi.org/10.1029/2011GB004198, 2012.
- Broecker, W. S., Peteet, D. M., & Rind, D. Does the ocean–atmosphere system have more than one stable mode of operation? Nature, 315(6014), 21-26, https://doi.org/10.1038/315021a0, 1985.
- Bubenshchikova, N., Nürnberg, D., & Tiedemann, R. Variations of Okhotsk Sea oxygen minimum zone: Comparison of foraminiferal and sedimentological records for latest MIS 12– 11c and latest MIS 2–1. Marine Micropaleontology, 121, 52-69, https://doi.org/10.1016/j.marmicro.2015.09.004, 2015.
- 11. Burke, A., & Robinson, L. F. The Southern Ocean's role in carbon exchange during the last deglaciation. science, 335(6068), 557-561, DOI: 10.1126/science.1208163, 2012.

12. Cartapanis, O., Tachikawa, K., & Bard, E. Northeastern Pacific oxygen minimum zone
 variability over the past 70 kyr: Impact of biological production and oceanic ventilation.
 Paleoceanography, 26(4), https://doi.org/10.1029/2011PA002126, 2011.

822

823

824

825

826

827 828

829

830

831

832

833

834

835

836

837 838

839

840 841

842

843 844

845

846 847

848

849

850

851

852

853

854

855

856 857

858

859

860 861

862

863 864

865

- 13. Casciotti, K. L. Nitrite isotopes as tracers of marine N cycle processes. Phil. Trans. R. Soc. A. 374:20150295, https://doi.org/10.1098/rsta.2015.0295, 2016.
- Chang, A. S., Pedersen, T. F., & Hendy, I. L. Effects of productivity, glaciation, and ventilation on late Quaternary sedimentary redox and trace element accumulation on the Vancouver Island margin, western Canada. Paleoceanography, 29(7), 730–746, https://doi.org/10.1002/2013PA002581, 2014.
- Chang, A. S., Pichevin, L., Pedersen, T. F., Gray, V., & Ganeshram, R. New insights into productivity and redox-controlled trace element (Ag, Cd, Re, and Mo) accumulation in a 55 kyr long sediment record from Guaymas Basin, Gulf of California. Paleoceanography, 30(2), 77-94, https://doi.org/10.1002/2014PA002681, 2015.
- Cheshire, H., & Thurow, J. High-resolution migration history of the Subtropical High/Trade Wind system of the northeastern Pacific during the last~ 55 years: Implications for glacial atmospheric reorganization. Paleoceanography, 28(2), 319-333, https://doi.org/10.1002/palo.20031, 2013.
- Choquel, C., Geslin, E., Metzger, E., Filipsson, H. L., Risgaard-Petersen, N., Launeau, P., Giraud, M., Jauffrais, T., Jesus, B., and Mouret, A.: Denitrification by benthic foraminifera and their contribution to N-loss from a fjord environment, Biogeosciences, 18, 327–341, https://doi.org/10.5194/bg-18-327-2021, 2021.
- 18. Clark, P. U., & Mix, A. C.: Ice sheets and sea level of the Last Glacial Maximum. Quaternary Science Reviews, 21(1-3), 1-7, https://doi.org/10.1016/S0277-3791(01)00118-4, 2002.
- Clark, P., Pisias, N., Stocker, T., Weaver, A. J.: The role of the thermohaline circulation in abrupt climate change. Nature 415, 863–869, https://doi.org/10.1038/415863a, 2002.
- Codispoti, L. A., Brandes, J. A., Christensen, J. P., Devol, A. H., Naqvi, S. W. A., Paerl, H. W., and Yoshinari, T.: The oceanic fixed nitrogen and nitrous oxide budgets: Moving targets as we enter the anthropocene? Sci. Mar. 65, 85–105, https://doi.org/10.17615/ksfx-e447, 2001.
- Dale, A. W., Sommer, S., Lomnitz, U., Bourbonnais, A. & Wallmann, K.: Biological nitrate transport in sediments on the Peruvian margin mitigates benthic sulfide emissions and drives pelagic N loss during stagnation events. Deep Res. I Oceanogr. Res. Pap. 112, 123–136, https://doi.org/10.1016/j.dsr.2016.02.013, 2016.
- Devol, A. H., Uhlenhopp, A. G., Naqvi, S. W. A., Brandes, J. A., Jayakumar, D. A., Naik, H., Gaurin, S., Codispoti, L. A., & Yoshinari, T.: Denitrification rates and excess nitrogen gas concentrations in the Arabian Sea oxygen deficient zone. Deep Sea Research Part I:
 Oceanographic Research Papers, 53(9), 1533-1547, https://doi.org/10.1016/j.dsr.2006.07.005, 2006.
- Dubois, N., Kienast, M., Kienast, S., Normandeau, C., Calvert, S. E., Herbert, T. D., & Mix, A.: Millennial-scale variations in hydrography and biogeochemistry in the Eastern Equatorial Pacific over the last 100 kyr. Quaternary Science Reviews, 30(1–2), 210–223, https://doi.org/10.1016/j.quascirev.2010.10.012, 2011.
- Dubois, N., Kienast, M., Kienast, S. S., & Timmermann, A.: Millennial-scale Atlantic/East Pacific Sea surface temperature linkages during the last 100,000 years. Earth and Planetary Science Letters, 396, 134–142, https://doi.org/10.1016/j.epsl.2014.04.008, 2014.
- Duplessy, J. C., Shackleton, N. J., Fairbanks, R. G., Labeyrie, L., Oppo, D., & Kallel, N.: Deepwater source variations during the last climatic cycle and their impact on the global deepwater circulation. Paleoceanography, 3 (3), 343–360, https://doi.org/10.1029/PA003i003p00343, 1988.

Emmer, E., & Thunell, R. C.: Nitrogen isotope variations in Santa Barbara Basin sediments:
 Implications for denitrification in the eastern tropical North Pacific during the last 50,000 years.
 Paleoceanography, 15(4), 377-387, https://doi.org/10.1029/1999PA000417, 2000.

870 871

872

873 874

875

876

877 878

879

880

881 882

883

884

885

886

887

888

889 890

891 892

893 894

895

896 897

898

899

900 901

902

903 904 905

906

907

908

909

910

911

912

913

914

- Erdem, Z., Schönfeld, J., Rathburn, A. E., Pérez, M. E., Cardich, J., & Glock, N.: Bottom-water deoxygenation at the Peruvian margin during the last deglaciation recorded by benthic foraminifera. Biogeosciences, 17(12), 3165-3182, https://doi.org/10.5194/bg-17-3165-2020, 2020
- 28. Evans, N., Tichota, J., Ruef, W., Moffett, J., & Devol, A.: Rapid Expansion of Fixed Nitrogen Deficit in the Eastern Pacific Ocean Revealed by 50-Year Time Series. Global Biogeochemical Cycles, 37(10), e2022GB007575, https://doi.org/10.1029/2022GB007575, 2023.
- Fontanier, C., Duros, P., Toyofuku, T., Oguri, K., Koho, K. A., Buscail, R., Grémare, A., Radakovitch, O., Deflandre, B., De Nooijer, L. J., Bichon, S., Goubet, S., Ivanovsky, A., Chabaud, G., Menniti, C., Reichart, G.-J., and Kitazato, H.: Living (stained) deep-sea foraminifera off hachinohe (NE Japan, western Pacific): environmental interplay in oxygendepleted ecosystems. J. Foraminifer. Res. 44, 281–299, https://doi.org/10.2113/gsjfr.44.3.281, 2014.
- Frölicher, T. L., Aschwanden, M. T., Gruber, N., Jaccard, S. L., Dunne, J. P., & Paynter, D.: Contrasting upper and deep ocean oxygen response to protracted global warming. Global biogeochemical cycles, 34(8), e2020GB006601, https://doi.org/10.1029/2020GB006601, 2020.
- Fu, W., Primeau, F., Keith Moore, J., Lindsay, K., & Randerson, J. T.: Reversal of increasing tropical ocean hypoxia trends with sustained climate warming. Global Biogeochemical Cycles, 32(4), 551-564, https://doi.org/10.1002/2017GB005788, 2018.
- 32. Galbraith, E. D., Kienast, M., Pedersen, T. F., & Calvert, S. E.: Glacial-interglacial modulation of the marine nitrogen cycle by high-latitude O₂ supply to the global thermocline. Paleoceanography, 19(4), https://doi.org/10.1029/2003PA001000, 2004.
- Ganeshram, R. S., & Pedersen, T. F.: Glacial-interglacial variability in upwelling and bioproductivity off NW Mexico: Implications for quaternary paleoclimate. Paleoceanography, 13(6), 634-645, https://doi.org/10.1029/98PA02508, 1998.
- Ganeshram, R. S., Pedersen, T. F., Calvert, S. E., & Murray, J. W.: Large changes in oceanic nutrient inventories from glacial to interglacial periods. Nature, 376(6543), 755-758, https://doi.org/10.1038/376755a0, 1995.
- Ganeshram, R. S., Pedersen, T. F., Calvert, S. E., McNeill, G. W., & Fontugne, M. R.: Glacial-interglacial variability in denitrification in the world's oceans: Causes and consequences. Paleoceanography, 15(4), 361-376, https://doi.org/10.1029/1999PA000422, 2000.
- Garcia H.E., Boyer, T. P., Baranova, O. K., Locarnini, R.A., Mishonov, A.V., Grodsky, A., Paver, C.R., Weathers, K.W., Smolyar, I.V., Reagan, J.R., Seidov, M.M., Zweng, D.: World Ocean Atlas 2018: product documentation, A. Mishonov, Technical Editor, NOAA Atlas NESDIS, 2019
- Glock, N., Erdem, Z., Wallmann, K., Somes, C. J., Liebetrau, V., Schönfeld, J., Gorb, S., & Eisenhauer, A.: Coupling of oceanic carbon and nitrogen facilitates spatially resolved quantitative reconstruction of nitrate inventories. Nat. Commun. 9, 1217, https://doi.org/10.1038/s41467-018-03647-5, 2018.
- 38. Glock, N., Eisenhauer, A., Milker, Y., Liebetrau, V., Schönfeld, J., Mallon, J., Sommer, S., & Hensen, C.: Environmental influences on the pore density of *Bolivina spissa* (Cushman). J. Foraminifer. Res. 41, 22–32, https://doi.org/10.2113/gsjfr.41.1.22, 2011.
- 39. Glock, N., Roy, A., Romero, D., Wein, T., Weissenbach, J., Revsbech, N. P., Høgslund, S., Clemens, D., Sommer, S., & Dagan, T.: Metabolic preference of nitrate over oxygen as an electron acceptor in foraminifera from the Peruvian oxygen minimum zone. Proc. Natl. Acad. Sci. U. S. A. 116, 2860–2865, https://doi.org/10.1073/pnas.18138871, 2019.

Glock, N., Schönfeld, J., Eisenhauer, A., Hensen, C., Mallon, J., & Sommer, S.: The role of benthic foraminifera in the benthic nitrogen cycle of the Peruvian oxygen minimum zone,
 Biogeosciences, 10, 4767–4783, https://doi.org/10.5194/bg-10-4767-2013, 2013.

919

920

921 922

923

924

925

926

927

928

929

930

931

932

933

934

935

936

937

938

939

940 941

942

943

944

945

946

947 948

949

950

951

952

953

954

955

956 957

958

959

960 961

- 41. Glock, N., Erdem, Z., & Schönfeld, J.: The Peruvian oxygen minimum zone was similar in extent but weaker during the Last Glacial Maximum than Late Holocene. Communications Earth & Environment, 3(1), 307, https://doi.org/10.1038/s43247-022-00635-y, 2022.
- Gomaa, F., Utter, D. R., Powers, C., Beaudoin, D. J., Edgcomb, V. P., Filipsson, H. L., Hansel, C.M., Wankel, S.D., Zhang, Y., & Bernhard, J. M.: Multiple integrated metabolic strategies allow foraminiferan protists to thrive in anoxic marine sediments. Science Advances, 7(22), eabf1586, DOI: 10.1126/sciadv.abf1586, 2021.
- Gorbarenko, S. A., Artemova, A. V., Goldberg, E. L., & Vasilenko, Y. P.: The response of the Okhotsk Sea environment to the orbital-millennium global climate changes during the Last Glacial Maximum, deglaciation and Holocene. Global and Planetary Change, 116, 76-90, https://doi.org/10.1016/j.gloplacha.2014.02.002, 2014.
- Govindankutty Menon, A., Davis, C.V., Nürnberg, D., Nomaki, H., Salonen, I., Schmiedl, G., & Glock, N.: A deep-learning automated image recognition method for measuring pore patterns in closely related bolivinids and calibration for quantitative nitrate paleo-reconstructions. Sci Rep 13, 19628, https://doi.org/10.1038/s41598-023-46605-y, 2023.
- Gray, W. R., Wills, R. C., Rae, J. W., Burke, A., Ivanovic, R. F., Roberts, W.H., Ferreira, D., &Valdes, P. J.: Wind-driven evolution of the North Pacific subpolar gyre over the last deglaciation. Geophysical Research Letters, 47(6), e2019GL086328, https://doi.org/10.1029/2019GL086328, 2020.
- Gruber, N.: The marine nitrogen cycle: overview and challenges. In D. G. Capone et al. (Eds.), Nitrogen in the marine environment, 2, 1-50, DOI: 10.1016/B978-0-12-372522-6.00001-3, 2008
- Hendy, I. L., Pedersen, T. F., Kennett, J. P., & Tada, R.: Intermittent existence of a southern Californian upwelling cell during submillennial climate change of the last 60 kyr. Paleoceanography, 19(3), https://doi.org/10.1029/2003PA000965, 2004.
- Herguera, J. C., Herbert, T., Kashgarian, M., & Charles, C.: Intermediate and deep-water mass distribution in the Pacific during the Last Glacial Maximum inferred from oxygen and carbon stable isotopes. Quaternary Sci. Rev., 29, 1228–1245, https://doi.org/10.1016/j.quascirev.2010.02.009, 2010.
- 49. Hess, A. V., Auderset, A., Rosenthal, Y., Miller, K. G., Zhou, X., Sigman, D. M., & Martínez-García, A.: A well-oxygenated eastern tropical Pacific during the warm Miocene. Nature, 619(7970), 521-525, https://doi.org/10.1038/s41586-023-06104-6, 2023.
- Holbourn, A., Kiefer, T., Pflaumann, U., & Rothe, S.: WEPAMA Cruise MD 122/IMAGES VII, Rapp. Campagnes Mer OCE/2002/01, Inst. Polaire Fr. Paul Emile Victor (IPEV), Plouzane. France. 2002.
- 51. Jaccard, S., Galbraith, E.: Large climate-driven changes of oceanic oxygen concentrations during the last deglaciation. Nature Geosci 5, 151–156, https://doi.org/10.1038/ngeo1352, 2012
- Kamp, A., Høgslund, S., Risgaard-Petersen, N., & Stief, P.: Nitrate storage and dissimilatory nitrate reduction by eukaryotic microbes. Front. Microbiol., 6, 1492, https://doi.org/10.3389/fmicb.2015.01492, 2015.
- Karstensen, J., & Quadfasel, D.: Formation of Southern Hemisphere thermocline waters: water mass conversion and subduction, J. Phys. Oceanogr., 32, 3020–3038, https://doi.org/10.1175/1520-0485(2002)032<3020:FOSHTW>2.0.CO;2, 2002.
- 54. Keeling, R. F., Kortzinger, A. & Gruber, N.: Ocean deoxygenation in a warming world. Ann.
 Rev.Mar. Sci. 2, 199–229, https://doi.org/10.1146/annurev.marine.010908.163855, 2010.

55. Keigwin, L. D.: Glacial-age hydrography of the far northwest Pacific Ocean.
 Paleoceanography, 13(4), 323-339, https://doi.org/10.1029/98PA00874, 1998.

967

968

969

970

971

972 973

974

975

976

977 978

979

980

981

982

983 984

985

986

987

988

989

990

991 992

993

994 995

996

997

998

999

1000

1001

1002

1003

1004

1005

1006 1007

1008

1009 1010

- Keigwin, L. D., & Jones, G. A.: Deglacial climatic oscillations in the Gulf of California. Paleoceanography, 5(6), 1009-1023, https://doi.org/10.1029/PA005i006p01009, 1990.
- 57. Kienast, S. S., Calvert, S. E., & Pedersen, T. F.: Nitrogen isotope and productivity variations along the northeast Pacific margin over the last 120 kyr: Surface and subsurface paleoceanography. Paleoceanography, 17(4), 7-1, https://doi.org/10.1029/2001PA000650, 2002
- Kienast, M., Higginson, M. J., Mollenhauer, G., Eglinton, T. I., Chen, M. T., & Calvert, S. E.:
 On the sedimentological origin of down-core variations of bulk sedimentary nitrogen isotope ratios. Paleoceanography, 20(2), https://doi.org/10.1029/2004PA001081, 2005.
- Koutavas, A., Demenocal, P. B., Olive, G. C., & Lynch-Stieglitz, J.: Mid-Holocene El Niño-Southern Oscillation (ENSO) attenuation revealed by individual foraminifera in eastern tropical Pacific sediments. Geology, 34(12), 993-996, https://doi.org/10.1130/G22810A.1, 2006.
- Kuhlmann, H., Freudenthal, T., Helmke, P., & Meggers, H.: Reconstruction of paleoceanography off NW Africa during the last 40,000 years: influence of local and regional factors on sediment accumulation. *Marine Geology*, 207(1-4), 209-224, https://doi.org/10.1016/j.margeo.2004.03.017, 2004.
- Kutzbach, J. E., & Wright Jr, H. E.: Simulation of the climate of 18,000 years BP: Results for the North American/North Atlantic/European sector and comparison with the geologic record of North America. Quaternary Science Reviews, 4(3), 147-187, https://doi.org/10.1016/0277-3791(85)90024-1, 1985.
- 62. Lam, P. & Kuypers, M. M.: Microbial nitrogen cycling processes in oxygen minimum zones. Ann. Rev. Mar. Sci. 3, 317–345, https://doi.org/10.1146/annurev-marine-120709-142814, 2011.
- 63. Leclaire, J., & Kerry, K.: Calcium carbonate and organic carbon stratigraphy of late Quaternary laminated and homogeneous diatom oozes from the Guaymas Slope, HPC Site 480, Gulf of California, in: Initial Reports of the Deep Sea Drilling Project, Vol. 64, edited by: Curray, J. R., Moore, D. G., et al., U.S. Government Printing Office, Washington, DC, 1263–1275, doi:10.2973/dsdp.proc.64.168.1982, 1982.
- Lembke-Jene, L., Tiedemann, R., Nürnberg, D., Gong, X., & Lohmann, G.: Rapid shift and millennial-scale variations in Holocene North Pacific Intermediate Water ventilation. Proceedings of the National Academy of Sciences, 115(21), 5365-5370, https://doi.org/10.1073/pnas.1714754115, 2018.
- Levin LA.: Oxygen minimum zone benthos: Adaptation and community response to hypoxia, in: Oceanography and Marine Biology: An Annual Review, Vol. 41, edited by: Gibson, R. N. and Atkinson, J. A., CRC Press, Boca Raton, FL, 1–45, doi:10.1201/9780203180570-3, 2003.
- Levin, L. A.: Manifestation, drivers, and emergence of open ocean deoxygenation. Annual review of marine science, 10(1), 229-260, https://doi.org/10.1146/annurev-marine-121916-063359, 2018.
- Li, N., Somes, C. J., Landolfi, A., Chien, C. T., Pahlow, M., & Oschlies, A.: Global impact of benthic denitrification on marine N₂ fixation and primary production simulated by a variablestoichiometry Earth system model, Biogeosciences, 21, 4361–4380, https://doi.org/10.5194/bg-21-4361-2024, 2024.
- 68. Liu, K. K., & Kaplan, I. R.: The eastern tropical Pacific as a source of 15N-enriched nitrate in seawater off southern California. Limnology and Oceanography, 34(5), 820-830, https://doi.org/10.4319/lo.1989.34.5.0820, 1989.
- 1012 69. Lourey, M. J., Trull, T. W., & Sigman, D. M.: Sensitivity of δ¹⁵N of nitrate, surface suspended
 1013 and deep sinking particulate nitrogen to seasonal nitrate depletion in the Southern Ocean.
 1014 Global Biogeochemical Cycles, 17(3), https://doi.org/10.1029/2002GB001973, 2003.

70. Martinez, P., & Robinson, R. S.: Increase in water column denitrification during the last
 deglaciation: the influence of oxygen demand in the eastern equatorial Pacific. Biogeosciences,
 7(1), 1-9, https://doi.org/10.5194/bg-7-1-2010, 2010.

1018

1019 1020

1021 1022

1023

1024

1025

1026 1027

1028

1029

1030

1031

1032

1033

1034

1035 1036

1037 1038

1039

1040

1041 1042

1043

1044 1045

1046

1047

1048 1049

1050

1051

1052 1053

1054

1055

1056 1057

1058

- Meckler, A. N., Ren, H., Sigman, D. M., Gruber, N., Plessen, B., Schubert, C. J., & Haug, G. H.: Deglacial nitrogen isotope changes in the Gulf of Mexico: Evidence from bulk sedimentary and foraminifera-bound nitrogen in Orca Basin sediments. Paleoceanography, 26(4), https://doi.org/10.1029/2011PA002156, 2011.
- 72. Meissner, K. J., Galbraith, E. D., & Völker, C.: Denitrification under glacial and interglacial conditions: A physical approach. Paleoceanography, 20(3), https://doi.org/10.1029/2004PA001083, 2005.
- Mollenhauer, G., Schneider, R. R., Müller, P. J., Spieß, V., & Wefer, G.: Glacial/interglacial variablity in the Benguela upwelling system: Spatial distribution and budgets of organic carbon accumulation. Global Biogeochemical Cycles, 16(4), 81-1, https://doi.org/10.1029/2001GB001488, 2002.
- Mollier-Vogel, E., Martinez, P., Blanz, T., Robinson, R., Desprat, S., Etourneau, J., Charlier, K., & Schneider, R.R.: Mid-holocene deepening of the Southeast Pacific oxycline. Glob. Planet. Change 172, 365–373, https://doi.org/10.1016/j.gloplacha.2018.10.020, 2019.
- 75. Mollier-Vogel, E., Leduc, G., Böschen, T., Martinez, P., & Schneider, R. R.: Rainfall response to orbital and millennial forcing in northern Peru over the last 18 ka. Quaternary Science Reviews, 76, 29-38, https://doi.org/10.1016/j.quascirev.2013.06.021, 2013.
- Montoya, J. P., Horrigan, S. G., & McCarthy, J. J.: Natural abundance of ¹⁵N in particulate nitrogen and zooplankton in the Chesapeake Bay. Marine Ecology Progress Series, 35-61, https://www.jstor.org/stable/24844633, 1990.
- 77. Moore, C.M., Mills, M.M., Arrigo, K.R., Berman-Frank, I., Bopp, L., Boyd, P.W., Galbraith, E.D., Geider, R.J., Guieu, C., Jaccard, S.L., & Jickells, T.D.: Processes and patterns of oceanic nutrient limitation. Nat. Geosci.6, 701–710, https://doi.org/10.1038/ngeo1765, 2013.
- Moretti, S., Auderset, A., Deutsch, C., Schmitz, R., Gerber, L., Thomas, E., Luciani, V., Petrizzo, M. R., Schiebel, R., Tripati, A., Sexton, P., Norris, R., D'Onofrio, R., Zachos, J., Sigman, D. M., Haug, G. H., & Martínez-García, A.: Oxygen rise in the tropical upper ocean during the Paleocene-Eocene Thermal Maximum. Science, 383(6684), 727-731, https://doi.org/10.1126/science.adh4893, 2024.
- Muratli, J. M., Chase, Z., Mix, A. C., & McManus, J.: Increased glacial-age ventilation of the Chilean margin by Antarctic Intermediate Water. Nature Geoscience, 3(1), 23-26, https://doi.org/10.1038/ngeo715, 2010.
- Naafs, B. D. A., Monteiro, F. M., Pearson, A., Higgins, M. B., Pancost, R. D., & Ridgwell, A.: Fundamentally different global marine nitrogen cycling in response to severe ocean deoxygenation. Proceedings of the National Academy of Sciences, 116(50), 24979-24984, https://doi.org/10.1073/pnas.1905553116, 2019.
- Narita, H., Sato, M., Tsunogai, S., Murayama, M., Ikehara, M., Nakatsuka, T., Wakatsuchi, M., Harada, N., & Ujiié, Y.: Biogenic opal indicating less productive northwestern North Pacific during the glacial ages. Geophysical Research Letters, 29(15), 22-1, https://doi.org/10.1029/2001GL014320, 2002.
- 82. Nürnberg, D., Böschen, T., Doering, K., Mollier-Vogel, E., Raddatz, J., & Schneider, R.: Sea surface and subsurface circulation dynamics off equatorial Peru during the last ~17 kyr, *Paleoceanography*, 30(7), 984–999, https://doi.org/10.1002/2014PA002706, 2015.
- 1060
 83. Ohkushi, K., Kennett, J. P., Zeleski, C. M., Moffitt, S. E., Hill, T. M., Robert, C., Beaufort, L.,
 2061
 2062
 2063
 2064
 2064
 2065
 2066
 2066
 2067
 2067
 2068
 2069
 2004
 2004
 2013
 2014
 2015
 2016
 2016
 2017
 2017
 2018
 2018
 2019
 2019
 2019
 2019
 2019
 2019
 2019
 2019
 2019
 2019
 2019
 2019
 2019
 2019
 2019
 2019
 2019
 2019
 2019
 2019
 2019
 2019
 2019
 2019
 2019
 2019
 2019
 2019
 2019
 2019
 2019
 2019
 2019
 2019
 2019
 2019
 2019
 2019
 2019
 2019
 2019
 2019
 2019
 2019
 2019
 2019
 2019
 2019
 2019
 2019
 2019
 2019
 2019
 2019
 2019
 2019
 2019
 2019
 2019
 2019
 2019
 2019
 2019
 2019
 2019
 2019
 2019
 2019
 2019
 2019
 2019
 2019
 2019
 2019
 2019
 2019
 2019
 2019
 2019
 2019
 2019
 2019
 2019</li

84. Okazaki, Y., Timmermann, A., Menviel, L., Harada, N., Abe-Ouchi, A., Chikamoto, M. O.,
 Mouchet, A., & Asahi, H.: Deepwater formation in the North Pacific during the last glacial
 termination. Science, 329(5988), 200-204, DOI: 10.1126/science.1190612, 2010.

1067

1068

1069 1070

1071

1072

1073

1074 1075

1076

1077 1078

1079

1080 1081

1082

1083

1084 1085

1086

1087

1088

1089

1090 1091

1092

1093

1094 1095

1096

1097

1098

1099

1100

1101 1102

1103

1104

1105 1106

1107

- 85. Orsi, W. D., Morard, R., Vuillemin, A., Eitel, M., Wörheide, G., Milucka, J., & Kucera, M.: Anaerobic metabolism of Foraminifera thriving below the seafloor, The ISME Journal, 14(10), 2580–2594, https://doi.org/10.1038/s41396-020-0708-1, 2020.
- Oschlies, A.: A committed fourfold increase in ocean oxygen loss. Nat Commun 12, 2307, https://doi.org/10.1038/s41467-021-22584-4, 2021.
- Pennington, J. T., Mahoney, K. L., Kuwahara, V. S., Kolber, D. D., Calienes, R., & Chavez, F.
 P.: Primary production in the eastern tropical Pacific: A review. *Progress in oceanography*, 69(2-4), 285-317, https://doi.org/10.1016/j.pocean.2006.03.012, 2006.
- Piña-Ochoa, E., Høgslund, S., Geslin, E., Cedhagen, T., Revsbech, N. P., Nielsen, L. P., Schweizer, M., Jorissen, F., Rysgaard, S., & Risgaard-Petersen, N.: Widespread occurrence of nitrate storage and denitrification among Foraminifera and Gromiida, *Proc. Natl. Acad. Sci.* U.S.A., 107(3), 1148–1153, https://doi.org/10.1073/pnas.0908440107, 2010a.
- 89. Piña-Ochoa, E., Koho, K. A., Geslin, E. & Risgaard-Petersen, N.: Survival and life strategy of the foraminiferan Globobulimina turgida through nitrate storage and denitrification. Mar. Ecol. Prog. Ser. 417, 39–49, https://doi.org/10.3354/meps, 2010b.
- Pospelova, V., Price, A. M., & Pedersen, T. F.: Palynological evidence for late Quaternary climate and marine primary productivity changes along the California margin. Paleoceanography, 30(7), 877-894. https://doi.org/10.1002/2014PA002728, 2015.
- Pride, C. J.: An evaluation and application of paleoceanographic proxies in the Gulf of California, Ph.D. dissertation, University of South Carolina, 1997.
- 92. Pride, C., Thunell, R., Sigman, D., Keigwin, L., Altabet, M., & Tappa, E.: Nitrogen isotopic variations in the Gulf of California since the last deglaciation: Response to global climate change. Paleoceanography, 14(3), 397-409, https://doi.org/10.1029/1999PA900004, 1999.
- Rae, J. W., Gray, W. R., Wills, R. C. J., Eisenman, I., Fitzhugh, B., Fotheringham, M., Shevenell, A. E., Taylor, B., & Burke, A.: Overturning circulation, nutrient limitation, and warming in the Glacial North Pacific, Sci. Adv., 6(50), eabd1654, https://doi.org/10.1126/sciadv.abd1654, 2020.
- Rae, J. W. B., Burke, A., Robinson, L. F., Foster, G. L., & Elliott, T.: CO₂ storage and release in the deep Southern Ocean on millennial to centennial timescales, Nature, 562, 569–573, https://doi.org/10.1038/s41586-018-0614-0, 2018.
- Rafter, P. A., Gray, W. R., Hines, S. K. V., Burke, A., Costa, K. M., Gottschalk, J., Hain, M. P., Rae, J. W. B., Southon, J. R., Walczak, M. H., Yu, J., Adkins, J. F., & DeVries, T.: Global reorganization of deep-sea circulation and carbon storage after the last ice age. Science Advances, 8(46), eabq5434, DOI: 10.1126/sciadv.abq5434, 2022.
- Rakshit, S., Glock, N., Dale, A. W., Armstrong, M. M., Scholz, F., Mutzberg, A., & Algar, C. K.: Foraminiferal denitrification and deep bioirrigation influence benthic biogeochemical cycling in a seasonally hypoxic fjord. *Geochim. Cosmochim. Acta*, 388, 268-282, https://doi.org/10.1016/j.gca.2024.10.010, 2025.
- Ren, H., Sigman, D. M., Chen, M. T., & Kao, S. J.: Elevated foraminifera-bound nitrogen isotopic composition during the last ice age in the South China Sea and its global and regional implications. Global Biogeochem. Cycles, 26(1) GB1020, https://doi.org/10.1029/2010GB004020, 2012.
- 98. Ren, H., Sigman, D. M., Chen, M. T., & Kao, S. J.: Elevated foraminifera-bound nitrogen isotopic composition during the last ice age in the South China Sea and its global and regional implications. Global Biogeochem. Cycles, 26(1) GB1020, https://doi.org/10.1029/2010GB004020, 2012.

- 1113
 99. Riechelson, H., Rosenthal, Y., Bova, S., & Robinson, R. S.: Southern Ocean biological pump
 1114 role in driving Holocene atmospheric CO₂: Reappraisal. Geophysical Research Letters, 51(4),
 1115 e2023GL105569, https://doi.org/10.1029/2023GL105569, 2024.
- 1116 100. Risgaard-Petersen, N., Langezaal, A. M., Ingvardsen, S., Schmid, M. C., Jetten, M. S. M., Op
 1117 den Camp, H. J. M., Derksen, J. W. M., Piña-Ochoa, E., Eriksson, S. P., Nielsen, L. P.,
 1118 Revsbech, N. P., Cedhagen, T., & van der Zwaan, G. J.: Evidence for complete denitrification
 1119 in a benthic foraminifer, *Nature*, 443, 93–96, https://doi.org/10.1038/nature, 2006.
 - Robinson, R. S., Sigman, D. M., DiFiore, P. J., Rohde, M. M., Mashiotta, T. A., & Lea, D. W.: Diatom-bound ¹⁵N/¹⁴N: New support for enhanced nutrient consumption in the ice age subantarctic. Paleoceanography, 20(3), https://doi.org/10.1029/2004PA001114, 2005.
 - Robinson, R. S., Mix, A., & Martinez, P.: Southern Ocean control on the extent of denitrification in the southeast Pacific over the last 70 ka. Quaternary Science Reviews, 26(1-2), 201-212, https://doi.org/10.1016/j.quascirev.2006.08.005, (2007).
 - Robinson, R. S., Martinez, P., Pena, L. D., & Cacho, I.: Nitrogen isotopic evidence for deglacial changes in nutrient supply in the eastern equatorial Pacific. Paleoceanography, 24(4), https://doi.org/10.1029/2008PA001702, 2009.
 - 104. Romanova, V., Lohmann, G., Grosfeld, K., & Butzin, M.: The relative role of oceanic heat transport and orography on glacial climate. Quaternary science reviews, 25(7-8), 832-845, https://doi.org/10.1016/j.quascirev.2005.07.007, 2006.
 - Russell, J. L., & Dickson, A. G.: Variability in oxygen and nutrients in South Pacific Antarctic intermediate water. Global biogeochemical cycles, 17(2), https://doi.org/10.1029/2000GB001317, 2003.
 - 106. Salvatteci, R., Gutiérrez, D., Field, D., Sifeddine, A., Ortlieb, L., Bouloubassi, I., Boussafir, M., Boucher, H., and Cetin, F.: The response of the Peruvian Upwelling Ecosystem to centennial-scale global change during the last two millennia, Clim. Past, 10, 715–731, https://doi.org/10.5194/cp-10-715-2014, 2014.
 - 107. Salvatteci, R., Gutiérrez, D., Sifeddine, A., Ortlieb, L., Druffel, E., Boussafir, M., & Schneider, R.: Centennial to millennial-scale changes in oxygenation and productivity in the Eastern Tropical South Pacific during the last 25,000 years. Quaternary Science Reviews, 131, 102-117, https://doi.org/10.1016/j.quascirev.2015.10.044, 2016.
 - Salvatteci, R., Schneider, R. R., Blanz, T., & Mollier-Vogel, E.: Deglacial to Holocene ocean temperatures in the Humboldt Current System as indicated by alkenone paleothermometry. Geophysical Research Letters, 46(1), 281-292, https://doi.org/10.1029/2018GL080634, 2019.
 - 109. Schlitzer, R.: Ocean Data View, odv.awi.de, 2023.

1120

1121

1122 1123

11241125

1126

1127

1128 1129

1130

1131 1132

1133 1134

1135

1136

11371138

1139

1140 1141

1142

1143 1144

1145

1146

1147 1148

1149

1150 1151

1152

1153

- Schmidtko, S., Stramma, L. & Visbeck, M.: Decline in global oceanic oxygen content during the past five decades. Nature 542, 335–339, https://doi.org/10.1038/nature21399, 2017.
- Scholz, F., McManus, J., Mix, A. C., Hensen, C., & Schneider, R. R.: The impact of ocean deoxygenation on iron release from continental margin sediments. *Nature Geoscience*, 7(6), 433-437, https://doi.org/10.1038/ngeo2162, 2014.
- 112. Scholz, F., Schmidt, M., Hensen, C., Eroglu, S., Geilert, S., Gutjahr, M., & Liebetrau, V.:
 1156 Shelf-to-basin iron shuttle in the Guaymas Basin, Gulf of California. Geochimica et
 1157 Cosmochimica Acta, 261, 76-92, https://doi.org/10.1016/j.gca.2019.07.006, 2019.
- Schubert, C. J., & Calvert, S. E.: Nitrogen and carbon isotopic composition of marine
 and terrestrial organic matter in Arctic Ocean sediments: implications for nutrient
 utilization and organic matter composition. Deep Sea Research Part I: Oceanographic
 Research Papers, 48(3), 789-810, https://doi.org/10.1016/S0967-0637(00)00069-8, 2001.

114. Seki, O., Ikehara, M., Kawamura, K., Nakatsuka, T., Ohnishi, K., Wakatsuchi, M.,
 1163 Narita, T., & Sakamoto, T.: Reconstruction of paleoproductivity in the Sea of Okhotsk
 1164 over the last 30 kyr. Paleoceanography, 19(1), https://doi.org/10.1029/2002PA000808,
 1165 2004.

- 115. Sigman, D. M., Altabet, M. A., Michener, R., McCorkle, D. C., Fry, B., & Holmes, R. M.: Natural abundance-level measurement of the nitrogen isotopic composition of oceanic nitrate: an adaptation of the ammonia diffusion method. Marine chemistry, 57(3-4), 227-242, https://doi.org/10.1016/S0304-4203(97)00009-1, (1997).
- 116. Skinner, L. C., Fallon, S., Waelbroeck, C., Michel, E., & Barker, S.: Ventilation of the deep Southern Ocean and deglacial CO₂ rise. Science, 328(5982), 1147-1151, DOI: 10.1126/science.118362, 2010.
- 117. Somes, C. J., Schmittner, A., Muglia, J., & Oschlies, A.: A three-dimensional model of the marine nitrogen cycle during the last glacial maximum constrained by sedimentary isotopes. Frontiers in Marine Science, 4, 108, https://doi.org/10.3389/fmars.2017.00108, 2017.
- Stramma, L., Johnson, G. C., Sprintall, J. & Mohrholz, V.: Expanding oxygen-minimum zones in the tropical oceans. Science 320(5876), 655–658, DOI: 10.1126/science.1153847, 2008.
- Stramma, L., Schmidtko, S., Levin, L. A. & Johnson, G. C.: Ocean oxygen minima expansions and their biological impacts. Deep-Sea Res. I Ocean. Res. Pap. 57(4), 587– 595, https://doi.org/10.1016/j.dsr.2010.01.005, 2010.
- 120. Studer, A. S., Mekik, F., Ren, H., Hain, M. P., Oleynik, S., Martínez-García, A., Jaccard, S. L., & Sigman, D. M.: Ice age-Holocene similarity of foraminifera-bound nitrogen isotope ratios in the eastern equatorial Pacific. Paleoceanography and Paleoclimatology, 36(5), e2020PA004063, https://doi.org/10.1029/2020PA004063, 2021.
- 121. Takano, Y., Ito, T., & Deutsch, C.: Projected centennial oxygen trends and their attribution to distinct ocean climate forcings. Global Biogeochemical Cycles, 32(9), 1329-1349, https://doi.org/10.1029/2018GB005939, 2018.
- 122. Taylor, M. A., Hendy, I. L., & Chappaz, A.: Assessing oxygen depletion in the Northeastern Pacific Ocean during the last deglaciation using I/Ca ratios from multiple benthic foraminiferal species. Paleoceanography, 32(8), 746-762, https://doi.org/10.1002/2016PA003062, 2017.
- 123. Ternois, Y., Kawamura, K., Keigwin, L., Ohkouchi, N., & Nakatsuka, T.: A biomarker approach for assessing marine and terrigenous inputs to the sediments of Sea of Okhotsk for the last 27,000 years. Geochimica et Cosmochimica Acta, 65(5), 791-802, https://doi.org/10.1016/S0016-7037(00)00598-6, 2001.
- 124. Tesdal, J.-E., Galbraith, E. D., & Kienast, M.: Nitrogen isotopes in bulk marine sediment: linking seafloor observations with subseafloor records, Biogeosciences, 10, 101–118, https://doi.org/10.5194/bg-10-101-2013, 2013.
- 125. Thunell, R. C., Sigman, D. M., Muller-Karger, F., Astor, Y., & Varela, R.: Nitrogen isotope dynamics of the Cariaco Basin, Venezuela. Global Biogeochemical Cycles, 18(3), https://doi.org/10.1029/2003GB002185, 2004.
- 126. Ujiié, H., & Ujiié, Y.: Late Quaternary course changes of the Kuroshio Current in the Ryukyu Arc region, northwestern Pacific Ocean. Marine Micropaleontology, 37(1), 23-40, https://doi.org/10.1016/S0377-8398(99)00010-9, 1999.
- 127. Van Geen, A., Fairbanks, R. G., Dartnell, P., McGann, M., Gardner, J. V., & Kashgarian, M.: Ventilation changes in the northeast Pacific during the last deglaciation. Paleoceanography, 11(5), 519-528, https://doi.org/10.1029/96PA01860, 1996.
- 1210 128. Voss, M., Bange, H. W., Dippner, J. W., Middelburg, J. J., Montoya, J. P., & Ward, B.:
 1211 The marine nitrogen cycle: recent discoveries, uncertainties and the potential relevance

of climate change, Philos. Trans. R. Soc. B, 368, 293–296,
 https://doi.org/10.1098/rstb.2013.0121, 2013.

- 129. Wada, E., & Hattori, A.: Nitrogen isotope effects in the assimilation of inorganic
 nitrogenous compounds by marine diatoms. Geomicrobiol. J. 1, 85–101,
 https://doi.org/10.1080/01490457809377725, 1978.
 - 130. Waelbroeck, C., Frank, N., Jouzel, J., Parrenin, F., Masson-Delmotte, V., & Genty, D.: Transferring radiometric dating of the last interglacial sea level high stand to marine and ice core records. Earth Planet. Sci. Lett., 265, 183–194, https://doi.org/10.1016/j.epsl.2007.10.006, 2008.
 - 131. Wallmann, K., Schneider, B., & Sarnthein, M.: Effects of eustatic sea-level change, ocean dynamics, and nutrient utilization on atmospheric pCO₂ and seawater composition over the last 130 000 years: a model study, Clim. Past, 12, 339–375, https://doi.org/10.5194/cp-12-339-2016, 2016.
 - 132. Wallmann, K., José, Y. S., Hopwood, M. J., Somes, C. J., Dale, A. W., Scholz, F., Grasse, P., & Oschlies, A.: Biogeochemical feedbacks may amplify ongoing and future ocean deoxygenation: a case study from the Peruvian oxygen minimum zone. Biogeochemistry, 159(1), 45-67, https://doi.org/10.1007/s10533-022-00908-w, 2022.
 - 133. Wang, Y., Hendy, I. L., & Thunell, R.: Local and remote forcing of denitrification in the northeast Pacific for the last 2,000 years. Paleoceanogr. Paleoclimatol, 34(8), 1517-1533, https://doi.org/10.1029/2019PA003577, 2019.
 - 134. Wang, Y., Hendy, I. L., & Zhu, J.: Expansion of the Southern California oxygen minimum zone during the early-to mid-Holocene due to reduced ventilation of the Northeast Pacific. Quaternary Sci. Rev., 238, 106326, https://doi.org/10.1016/j.quascirev.2020.106326, 2020.
 - 135. White, A. E., Foster, R. A., Benitez-Nelson, C. R., Masqué, P., Verdeny, E., Popp, B. N., Arthur, K.E., & Prahl, F. G.: Nitrogen fixation in the Gulf of California and the eastern tropical North Pacific. Prog. Oceanogr., 109, 1-17, https://doi.org/10.1016/j.pocean.2012.09.002, 2013.
 - 136. Woehle, C., Roy, A.-S., Glock, N., Wein, T., Weissenbach, J., Rosenstiel, P., Hiebenthal, C., Michels, J., Schönfeld, J., & Dagan, T.: et al. A Novel Eukaryotic Denitrification Pathway in Foraminifera. Curr. Biol. 28, 2536-2543.e5, https://doi.org/10.1016/j.cub.2018.06.027, 2018.
 - 137. Woehle, C., Roy, A., Glock, N., Michels, J., Wein, T., Weissenbach, J., Romero, D., Hiebenthal, C., Gorb, S. N., Schönfeld, J., & Dagan, T.: Denitrification in foraminifera has an ancient origin and is complemented by associated bacteria, Proc. Natl. Acad. Sci. U.S.A. 119 (25) e2200198119, https://doi.org/10.1073/pnas.2200198119, 2022.
 - 138. Yamamoto, A., Abe-Ouchi, A., Shigemitsu, M., Oka, A., Takahashi, K., Ohgaito, R., & Yamanaka, Y.: Global deep ocean oxygenation by enhanced ventilation in the Southern Ocean under long-term global warming. Global Biogeochemical Cycles, 29(10), 1801-1815, https://doi.org/10.1002/2015GB005181, 2015.